

STUDENTS' SPACE ASSOCIATION
THE FACULTY OF POWER AND AERONAUTICAL ENGINEERING
WARSAW UNIVERSITY OF TECHNOLOGY



CRITICAL DESIGN REVIEW

Attitude Determination and Control System

November 2016

Issue no. 1

	PW-Sat2	Critical Design Review	
	2016-11-30	Attitude Determination and Control System	
	Phase C		

Changes

Date	Changes	Pages/Section	Responsible
2016-11-30	First issue of the document	- ch. 6, 7, 9 ch. 4 -	Inna Uwarowa Paweł Jaworski Mateusz Zarudzki Dominik Roszkowski

Published by

Students' Space Association

Warsaw University of Technology, 2016

This work is licensed on CC BY-NC 3.0

Project logo by Krzysztof Karaś

Artist's impressions by Marcin Świetlik

Quote as: PW-Sat2 Team, *Phase C Documentation – Critical Design Review – Attitude Determination and Control System*, Students' Space Association, Warsaw University of Technology, pw-sat.pl 2016

	PW-Sat2	Critical Design Review	
	2016-11-30		
	Phase C	Attitude Determination and Control System	

Table of contents

1	Introduction	7
1.1	Document structure	7
1.2	Reference Documents	8
1.3	Applicable Project Documents.....	9
1.4	Document Contributors.....	9
2	Previous phases review	10
2.1	Introduction.....	10
2.2	Phase A	10
2.3	Phase B	11
3	ADCS Requirements	12
4	Hardware Description	14
4.1	Actuators	14
4.1.1	<i>Magnetorquers</i>	14
4.2	Sensors	15
4.2.1	<i>Sun Sensor</i>	15
4.2.2	<i>Magnetometer</i>	18
4.2.3	<i>Gyroscopes</i>	18
4.3	Conclusions.....	19
5	ADCS Architecture	20
5.1	Determination	21
5.2	Control	21
5.3	ADCS Modes.....	21
6	Design Analysis	23
6.1	Extended Kalman Filter	23
6.1.1	<i>Architecture</i>	24
6.2	Attitude Control	31
6.2.1	<i>Magnetorquers</i>	31
6.2.2	<i>Detumbling Control Mode</i>	32

	PW-Sat2	Critical Design Review	
	2016-11-30		
	Phase C	Attitude Determination and Control System	

6.2.3	<i>Sun Pointing Control Mode</i>	33
7	Simulation Results	36
7.1.1	<i>Case 1</i>	37
7.1.2	<i>Case 2</i>	43
8	ADCS Test Campaign	48
8.1	Hardware testing	48
8.1.1	<i>Sensors</i>	48
8.1.2	<i>Actuators</i>	51
8.2	Software	52
8.2.1	<i>Matlab</i>	52
9	Conclusions	54
10	Future Work	55
Appendix A	Coordinate systems	56
A.1	ECI – Earth Centred Inertial	56
A.2	ORF – Orbital Reference Frame	56
A.3	SBRF – Satellite’s Body Reference Frame	57

	PW-Sat2	Critical Design Review	
	2016-11-30		
	Phase C	Attitude Determination and Control System	

List of figures

Figure 4-1 iMTQ Board	14
Figure 5-1 ADCS Block Diagram for Sun Pointing Mode.....	20
Figure 6-1 Underactuation of the magnetic control system.....	32
Figure 6-2 Spin stabilization around the satellite's X axis.....	33
Figure 7-1 Case 1: Satellite's angular rate in SBRF.....	39
Figure 7-2 Case 1: Sun Pointing Error	39
Figure 7-3 Case 1: Control magnetic dipole.....	40
Figure 7-4 Case 1: EKF performance. Sun angles and angular rate estimation errors.....	41
Figure 7-5 Case 1: EKF performance. Sun angles and angular rate residuals (innovations)	42
Figure 7-6 Case 2: Satellite's angular rate in SBRF.....	44
Figure 7-7 Case 2: Sun Pointing Error	44
Figure 7-8 Case 2: Control magnetic dipole.....	45
Figure 7-9 Case 2: EKF performance. Sun angles and angular rate estimation errors.....	46
Figure 7-10 Case 2: EKF performance. Sun angles and angular rate residuals (innovations)	47
Figure 9-1 Reference Sun Sensor wiring test	49
Figure 9-2 Sun Sensor test stand	50
Figure 9-3 Test table at Rzeszów University of Technology.....	51

List of figures in Appendices

Figure A-1 ECI inertial and ORF orbital coordinate systems	56
Figure A-2 Body axes definition [X-;Y-;Z-]	57
Figure A-3 Body axes definition [X-;Y+;Z-]	58
Figure A-4 Body axes definition [X+;Z-].....	58
Figure A-5 Body axes definition [X+;Y-;Z+].....	59

List of tables

Table 3-1 ADCS Requirements	12
Table 4-1 iMTQ Specification.....	15
Table 4-2 SSBV Sun Sensor Specification.....	17
Table 5-1 ADCS on-orbit sequence.....	22
Table 6-1 Sensors Outage Handling.....	30
Table 7-1 Simulation's parameters	36

	PW-Sat2	Critical Design Review	
	2016-11-30		
	Phase C	Attitude Determination and Control System	

Abbreviated terms

ADCS	Attitude Determination and Control System
COMM	Communication subsystem
CMOS	Complementary Metal-Oxide Semiconductor
COTS	Commercial Off-The-Shelf
CSS	Coarse Sun Sensor
DT	Deployment Team
ECI	Earth Centered Inertial
EKF	Extended Kalman Filter
EM	Engineering Model
EPS	Electrical Power System
ESA	European Space Agency
FM	Flight Model
FOV	Field of View
GS	Ground Station
I2C	Inter-Integrated Circuit
IGRF	International Geomagnetic Reference Field
LEO	Low Earth Orbit
MA	Mission Analysis
MEKF	Multiplicative Extended Kalman Filter
MDR	Mission Definition Review
MEMS	Micro Electro-Mechanical Systems
MLI	Multi-Layer Insulation
MTM	Magnetometer
PD	Proportional – Derivative
PDR	Preliminary Design Review
PSD	Position Sensitive Device
PWM	Pulse-Width Modulation
SBRF	Satellite Body Reference Frame
SGP	Simplified General Perturbations
SC	Spacecraft
SKA	Studenckie Koło Astronautyczne (Students' Space Association)
SSO	Sun-Synchronous Orbit
SW	Software
TBC	To Be Continued
TBD	To Be Defined
TRIAD	TRIaxial Attitude Determination
WUT	Warsaw University of Technology

	PW-Sat2	Critical Design Review	
	2016-11-30		
	Phase C	Attitude Determination and Control System	

Mathematical notation used in this document is described below:

1. Bold font describes vector, e.g. \mathbf{a}
2. Bold font, capital letter and the underline describe matrix, e.g. $\underline{\mathbf{B}}$, however the matrix $\underline{\mathbf{A}}$ is reserved for orthogonal transformation matrices
3. Left superscript describes the coordinate system in which the vector is expressed, e.g. ${}^s\mathbf{a}$
 - 3.1. ‘i’ – ECI inertial frame
 - 3.2. ‘o’ – ORF orbital frame
 - 3.3. ‘s’ – SBRF satellite’s body frame
4. Matrix ${}^s\underline{\mathbf{A}}$ describes the rotation from coordinate frame denoted ‘i’ to the ‘s’ coordinate frame
5. Quaternion ${}^i\mathbf{q}$ describes the rotation from coordinate frame denoted ‘i’ to the ‘s’ coordinate frame
6. Transformation matrix formed from a quaternion ${}^i\mathbf{q}$ is denoted ${}^i\underline{\mathbf{A}}(\mathbf{q})$
7. The angular rate vector of a ‘s’ coordinate system relative to ‘i’ coordinate system is denoted $\boldsymbol{\omega}_{s/i}$
8. The element in i -th row and j -th column in matrix $\underline{\mathbf{B}}$ is denoted $\underline{\mathbf{B}}(i,j)$
9. Skew-symmetric 3x3 matrix formed with the 3x1 vector’s \mathbf{a} components is denoted $[\mathbf{a} \times]$

	PW-Sat2	Critical Design Review	
	2016-11-30	Attitude Determination and Control System	
	Phase C		

1 INTRODUCTION

The main purpose of this document is to present current development of the ADCS subsystem for PW Sat2 CubeSat. The document begins with the verification of the requirements and architecture of the ADCS in previous Phase B [1] report from May 2015. Relevant changes are presented.

The major task of ADCS is pointing the deployed solar panels towards the Sun within predetermined accuracy. Thus the estimation of the attitude with the presence of noise is required. Second task of attitude control system is detumbling, i.e. deceleration satellite's rotational motion after P-POD deployment.

Since April 2014 [2] major effort was put on testing the algorithms for attitude determination and estimation with the presence of expected sensors' noise. Moreover, attitude control strategy was changed taking into account expected disturbance torques acting on the satellite on orbit. To verify proposed approach, the simulation software was developed which utilizes environmental models, satellite dynamics and kinematics, sensors and actuators emulation with expected noise. Results for given attitude estimation and control algorithms are presented and thoroughly discussed.

The team also chose the sensors and actuators necessary for meeting the functional requirements. However, the final decision about the exact models of sensors has not been done. In the simulation software, one can modify the magnitude of sensors' errors as inputs and obtain desired performance of sensors in order to meet the overall ADCS requirements.

The comparison of several types of sensors is presented and possible trade-offs are discussed. Since purchased sensors will be COTS, low-cost, based on MEMS technology, choosing the sensors which worked properly on previous CubeSat missions is emphasized.

Since the phase B report, possible configuration of photodiodes and the algorithms for determining Sun vector based on relative photodiodes measurements have been derived. However, during the algorithm development it appeared the photodiodes are not necessary and the magnetometer mounted on iTMQ board is more accurate and easier to communicate with. Therefore both photodiodes set and external magnetometer had been removed from ADCS hardware and software.

1.1 DOCUMENT STRUCTURE

Chapter 2 revises assumptions and work done during previous phases.

Chapter 3 describes fundamental requirements for all ADCS subsystems.

	PW-Sat2	Critical Design Review	
	2016-11-30		
	Phase C	Attitude Determination and Control System	

Chapter 4 contains description of actuators (Magnetorquers) and sensors (Sun Sensor, Magnetometers, Gyroscopes, Photodiodes) used in ADCS system of PW-Sat2.

Chapter 5 describes the ADCS architecture in terms of determination, control and ADCS modes.

Chapter 6 provides design analysis of system.

Chapter 7 presents the simulation results

Chapter 8 summarizes plan for test campaign for ADCS and related software.

Chapter 9 concludes the document.

Chapter 10 lists planned tasks and future activities.

1.2 REFERENCE DOCUMENTS

1.3

- [1] PW-Sat2, „Preliminary Design Review,” Students' Space Association, Warsaw, 2015.
- [2] PW-Sat2, „Preliminary Requirements Review,” Students' Space Association, Warsaw, 2014.
- [3] Innovative Solutions in Space (ISIS), "Magnetorquer Board User Manual, v.1.1," 2011.
- [4] SSBV, "Cubesat Sun Sensor Datasheet".
- [5] Sensixs Design B.V., "XEN1210 Magnetic Sensor Datasheet, v.1.7," 2013.
- [6] A. Slavinskis, U. Kvell, E. Kulu, I. Sunter, H. Kuuste, S. Latt, K. Voormansik and M. Noorma, "High Spin Rate Controller for nanosatellites," *Acta Astronautica*, no. 95, 2014.
- [7] PW-Sat2, „Mission Definition Review,” Students' Space Association, Warsaw, 2013.
- [8] G. Michalareas, S. B. Gabriel and E. Rogers, Spacecraft Attitude Estimation based on Magnetometer Measurements and the Covariance Intersection Algorithm, University of Southampton.
- [9] J. F. Kasper and V. Kasper, Attitude Determination and Control System for AAUSat3 (Master Thesis), Aalborg University , 2010.
- [10] J. C. Springman and J. W. Cutler, Photodiodes Placement & Algorithms for CubeSat Attitude Determination,, CubeSat Developer's Workshop, 2012.
- [11] F. L. Markley i J. L. Crassidis, Fundamentals of Spacecraft Attitude Determination and Control, Springer, 2014.
- [12] OSRAM, "SFH2430 Photodiode Datasheet v.1.0".
- [13] J. C. Springman and J. W. Cutler, "Initial Attitude Analysis of the RAX Satellite".
- [14] ESL, "CubeMagnetometer - Interface Control Document".
- [15] D. Air and S. Claridge, "Surface Albedo Estimation".

	PW-Sat2	Critical Design Review	
	2016-11-30	Attitude Determination and Control System	
	Phase C		

- [16] P. Furła, M. Kwas i J. Toruniewska, „Słonecznik – Symulator Słońca do Komory Próżniowej, Sprawozdanie merytoryczne,” Warszawa, 2012.
- [17] A. Łukasik, „Construction of a test stand for satellite’s attitude determination system tests (Bachelor Thesis),” Warsaw University of Technology, Warsaw , 2014.
- [18] T. S. Kelso, "Validation of SGP4 and IS-GPS-200D Against GPS Precision Ephemerides," in *17th AAS/AIAA Space Flight Mechanics Conference*, Arizona, 2007.
- [19] International Association of Geomagnetism and Aeronomy, Working Group V-Mod, "International Geomagnetic Reference Field: the eleventh generation," *Geophysical Journal International*, September 2010.
- [20] M. J. Sidi, *Spacecraft Dynamics & Control, A Practical Engineering Approach*, Cambridge University Press, 1997.
- [21] AzurSpace , "28% Triple Junction GaAs Solar Cell Datasheet," 2012.
- [22] C. Fruh, T. M. Kelecy and M. K. Jah, "Attitude Dynamics Simulation of MLI Space Debris Objects in Geosynchronous Earth Orbits".

1.4 APPLICABLE PROJECT DOCUMENTS

- [PW-Sat2-C-00.00-Overview-CDR] – the overview of the PW-Sat2 Phase C
- [PW-Sat2-B-01.00-ADCS-PDR] – overview of PW-Sat2 ADCS in Phase B

1.5 DOCUMENT CONTRIBUTORS

This document and any results described were prepared solely by PW-Sat2 project team members.

	PW-Sat2	Critical Design Review	
	2016-11-30	Attitude Determination and Control System	
	Phase C		

2 PREVIOUS PHASES REVIEW

2.1 INTRODUCTION

This sections presents the activities performed during previous phases to give the reader opportunity to follow the development path of the authors.

2.2 PHASE A

The following problems from Phase A Report have been put into question and possible solutions have been proposed during Phase B:

- Magnetorquers are not able to stabilize the attitude in ECI inertial frame when expected disturbance torques are considered. Using the reaction wheel is not considered because of mass, financial and volume constraints. Spin stabilization about the axis perpendicular to the deployed solar panels which is simultaneously collinear with the Sun direction has been examined in detail and proves to be feasible.
- With spin stabilization, the accuracy of Sun pointing can be significantly enhanced. Based on the simulations' results, Sun pointing error at the level of 5 degrees is feasible.
- Taking the pictures of the Earth is not considered, thus Nadir Pointing is not necessary.
- Accuracy of the magnetometer is crucial, so the team considers using magnetometer outside the CubeSat, on the deployable boom. This will make the measurements less sensitive to the magnetic disturbances generated by the on-board electronics.
- Simplicity of the algorithms and the system architecture is important. Number of ADCS modes has been minimized to 4 and transitions has been simplified. Also, number of photodiodes have to be minimized, even at the expense of not covering whole attitude sphere¹. Kalman filter can still estimate the attitude with only one reference measurement from the magnetometer, which takes place in eclipse when no photodiodes' outputs are available.

¹ At least three photodiodes measurements are necessary to determine Sun direction using deterministic method. The normals of the photodiodes cannot be collinear. When the attitude sphere is fully covered, at least 3 photodiodes are illuminated for arbitrary Sun direction.

	PW-Sat2	Critical Design Review	
	2016-11-30		
	Phase C	Attitude Determination and Control System	

- The adaptation of the control gain in B-dot algorithm for detumbling mode in real-time applications is not considered. Constant gain gives satisfactory results, thus making the algorithm more complex should be avoided.

Detailed changes are presented in the following chapters.

2.3 PHASE B

The following problems from Phase B Report have been put into question and possible solutions have been proposed during Phase B and C:

- There were several sensors discussed to use in the previous phase. The final chose of the ADCS hardware has been made.
- The exact ADCS architecture had been determined and verified, the algorithms are in the process of rewriting on the OBC's microcontroller.
- The TLE algorithm for orbit propagator is under verification.
- The work under the ADCS telemetry and telecommand data structure is in progress. The ADCS modes description and the conditions to transition between them had been defined. The transitions will be programmed on OBC as well.

	PW-Sat2	Critical Design Review	
	2016-11-30	Attitude Determination and Control System	
	Phase C		

3 ADCS REQUIREMENTS

Taking into account changes in ADCS design approach, ADCS requirements have been refined and clarified in Phase C.

The major performance requirements refer to the Sun pointing error and time of detumbling. Sensors' errors such as noise, bias, drift and temperature sensitivity contribute mostly to the whole system performance. However, the team cannot afford high precision sensors due to the financial and volume constraints. The error of attitude determination influence the control error. Based on the other subsystems requirements, simulation results presented in chapter 7 and the currently on-orbit CubeSats with similar ADCS architecture, the requirements are stated. The reader should take into account that some of these values can be changed.

Table 3-1 below presents the summary of the ADCS requirements for both software and hardware. In terms of hardware - power, electrical and thermal requirements have not been examined, rather the performance has been emphasized. In next chapters, most requirements are explained in detail.

Table 3-1 ADCS Requirements

Requirement	Value	Unit
Software & General		
Control		
Sun pointing error with 2 coils working (>96% maximum solar energy)	15	deg
Detumbling possible from (angular rate vector norm) with 2 coils working	60	deg/s
Detumbling time for above condition	4	orbits
Autonomous detumbling from predetermined threshold	TBD	deg/s
control and determination algorithms must be able to run on Hercules TMS570	-	-
calculation time for one iteration during Detumbling	<20	ms
calculation time for one iteration during Sun Pointing (determination & control)	<150	ms
moment of inertia ratio about satellite X axis and Y axis	1.1	-
Determination		
attitude knowledge error in daylight (norm of small rotation vector)	<12	deg
Hardware		
Magnetotorquers		
magnetic moment error of command value on each axis for operating temperature conditions	5 (3 σ)	%
switched off when magnetometer takes measurements	-	-

	PW-Sat2	Critical Design Review	
	2016-11-30		
	Phase C	Attitude Determination and Control System	

supply voltage	5	V
able to identify fault coil and isolate it from other subsystems components	-	-
Gyroscopes		
random noise	<0.5	deg/ \sqrt{s}
bias instability	<0.006	deg/ $\sqrt{s^3}$
scale factors & misalignments elements errors	<0.03 (σ)	-
supply voltage	3.3	V
Magnetometers		
random noise	<100 (σ)	nT
at least one redundant magnetometer is required	-	-
able to identify fault MTM and isolate it from other subsystems components	-	-
constant biases on each axis	<1000	nT
scale factors & misalignments elements errors	<0.03 (σ)	-
angle between output and true magnetic field vector	<2.5 (σ)	deg
supply voltage	3.3	V
sampling rate	>5	Hz

	PW-Sat2	Critical Design Review	
	2016-11-30	Attitude Determination and Control System	
	Phase C		

4 HARDWARE DESCRIPTION

In this chapter, the choice of hardware is described. Each element is proven to be necessary. Detailed parameters of several sensors are presented. The necessity of redundancy is examined.

4.1 ACTUATORS

The team did not consider the possibility of using even single reaction wheel due to financial, mass and volume constraints. Thus, it was necessary to come up with the control strategy utilizing only set of 3 perpendicular electromagnetic coils called magnetorquers. Further details on control approach are discussed in chapter 6.2. Simulation results prove that magnetorquers and spin stabilisation controller let the solar panels point the Sun with very good accuracy. Magnetorquers are widely used to detumble satellite after P-POD deployment. Since Sun tracking and detumbling are major tasks of ADCS, magnetorquers as the only actuators have been proven sufficient and thus chosen.

4.1.1 MAGNETORQUERS

Set of 3 perpendicular electromagnetic coils was purchased from ISIS (Innovative Solutions in Space). The board comprises of 2 rods and 1 air core. Temperature sensors and magnetometer are included together with control module applying PWM signal to the coils. Above elements are fabricated on single PCB and supports I2C bus.

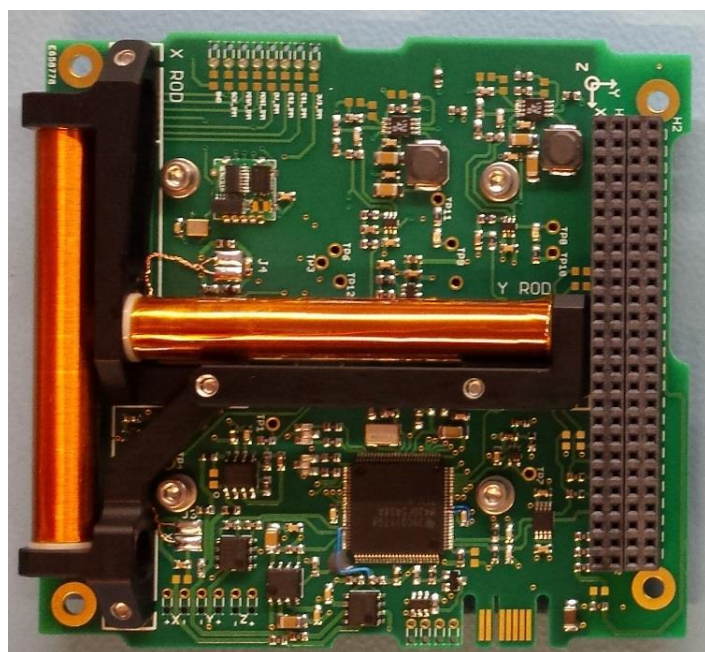


Figure 4-1 iMTQ Board

	PW-Sat2	Critical Design Review	
	2016-11-30		
	Phase C	Attitude Determination and Control System	

The figure above shows X & Y torque rods and I2C bus connector on the right. The Z air core is placed on the bottom side of the PCB. Table below shows overall specification of iMTQ [3].

Table 4-1 iMTQ Specification

Parameter	Value	Comment
Nominal magnetic dipole for torque rods (X, Y)	0.2 Am ²	5 V
Nominal magnetic dipole for air core (Z)	0.24 Am ²	5 V
Actuator power for rods (X, Y)	0.2 W	5 V, 20°C, 0.2 Am ²
Actuator power for air core (Z)	0.68 W	5 V, 20°C, 0.24 Am ²
Temperature sensor current consumption	<150 uA	-
Operational temperature range	-40 to +70°C	-
Mass	194 g	-

4.2 SENSORS

In detumbling mode the magnetometer is used to get an information about the rotation of the satellite. Only the information from the magnetometer is used in the control law. Such approach is called B-Dot algorithm and refers to the change of the Earth's magnetic field as a source of information about satellite's rotation. Indication from the on-board gyroscopes is used to track the rotation vector magnitude and assess the detumbling algorithm performance. Then the overall magnitude of the angular rate vector drops below a defined threshold, the detumbling mode is turned off. The control law is simple and robust. Further details on B-Dot algorithm can be found in chapter 6.2.2.

In Sun Pointing mode the algorithm will rely on the measurement from the Sun Sensor and gyroscopes. In order to filter the noise and increase the accuracy, sensor indications are fused with a specially designed Kalman Filter. In the B-phase of the documentation, photodiodes were also used in order to initialise the Kalman Filter regardless of the initial attitude of the satellite. After additional set of simulations, it was decided that the photodiodes will be omitted in order to simplify the ADCS system design from the hardware point of view. The goal of the Sun Pointing mode is to point the satellite towards the sun so that the solar panels can maximise the electrical energy they provide.

4.2.1 SUN SENSOR

In order to start sun pointing mode it is required to initialise Kalman Filter with an initial estimate about the satellite attitude with respect to the sun. Purchase of 6 fine Sun Sensors would be the best solution because regardless of the satellite's attitude the sun would be visible by at least one of them. That would allow for accurate estimate of the initial state. However, due to the financial constraints, the team is not able to purchase 6 fine Sun Sensors. Instead, purchasing an use of photodiodes for state initialisation was investigated. Photodiodes placed at angles can provide information about the Sun direction. However, the accuracy is low and the

	PW-Sat2	Critical Design Review	
	2016-11-30		
	Phase C	Attitude Determination and Control System	

advantages of such approach are not obvious – especially because additional hardware complicates the design. Another idea to wait until the disturbance moments rotate the satellite so that the sun is within the field-of-view of the single Sun Sensor was proposed. The Sun Sensor should be placed on the X+ surface of the satellite – the surface which solar panels are attached to. The question remains, how long would it take before the satellite is rotated so that the sun is within the FOV of the Sun Sensor. In order to analyse this idea a Monte Carlo simulation based on 1000 samples of initial attitude was performed. The results of this simulation are presented in the Figure 4-2.

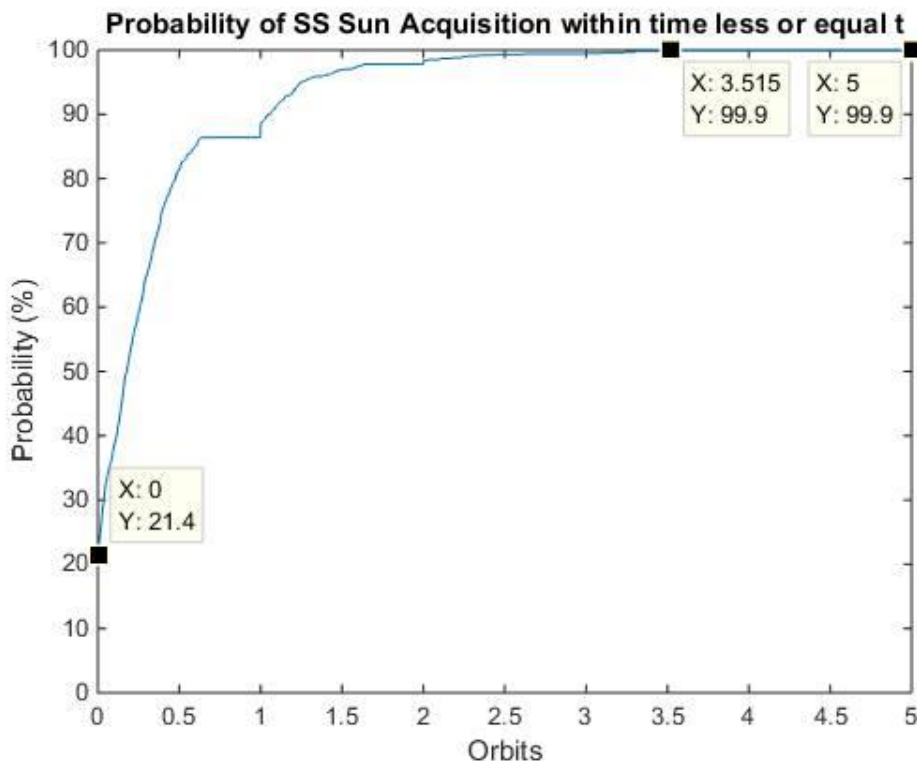


Figure 4-2 Monte Carlo simulation results

Each simulation was started with a random satellite attitude with respect to the Sun and ended when the Sun appeared in the FOV of the Sun Sensor and stayed visible for at least 20 seconds. The vertical axis shows the probability that the Sun is within the FOV of the SS after the number of orbits (horizontal axis) was completed by the PW-Sat2. As the chosen Sun Sensor covers one fourth of the sphere, nearly 25% of the simulations were finished for the number of orbits approximately equal to zero. The value 21.4% would approach 25% when the number of Monte Carlo simulations were increased. Horizontal lines in the plot represent the eclipse periods when, even if the satellite changes its attitude it is not possible to capture the Sun. According to the simulation results, around 95% of the simulations were finished after about 1.5 orbits (around 140 min) while almost all of them (99.9%) were finished before 3.5 orbits (around 335 min).

The analysis showed that statistically the satellite would not need big amount of time to obtain an attitude where Sun is visible by the Sun Sensor. Based on the result of the mentioned analysis it was decided that one Sun

	PW-Sat2	Critical Design Review	
	2016-11-30		
	Phase C	Attitude Determination and Control System	

Sensor located on the X+ face of the satellite will be used without any additional photodiodes. Such approach should allow for good performance of the Sun Pointing algorithm and requires minimal amount of hardware on the satellite. CMOS PSD Sun Sensor from SSBV was chosen as a reference sun sensor that will be used in the satellite. Table 4-2 shows specification of this Sun Sensor [4]. The sensor is presented in the Figure 4-3.

Table 4-2 SSBV Sun Sensor Specification

Parameter	Value
Field of View (FoV)	+/-57°
Accuracy	<0.5°
Update rate	>10 Hz
Operating temperature range	-25 to +50 °C
Supply voltage	5 V
Mass	< 5g
Power	<10 mA

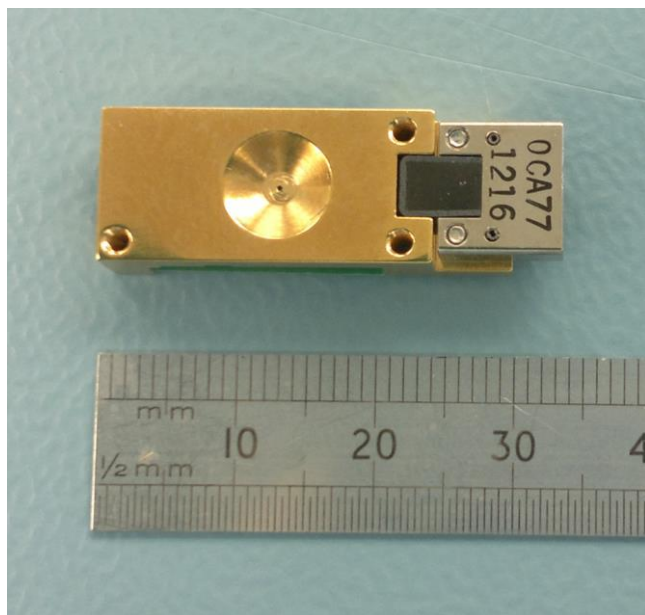


Figure 4-3 SSBV Sun Sensor

The sensor outputs four analogue voltages that are related to incident angle of sunlight in the horizontal and vertical directions [4]. 12bit Analogue to Digital Converted ADC128S102 from Texas Instruments will be used to convert those voltages into digital values and through a small additional microcontroller the attitude information will be sent to the OBC. The Sun Sensor is calibrated by the manufacturer and the calibration parameters are given in so called End Item Data Package (EIDP) as specified in the Interface Control Document[12] of this Sun Sensor.

	PW-Sat2	Critical Design Review	
	2016-11-30		
	Phase C	Attitude Determination and Control System	

For proper interpretation of the sensor's data it is important to distinguish Earth's albedo with the Sun. This is done based on some threshold voltage levels given by the Sun Sensor. It is assumed that Sun is within the FoV of the sensor if the voltage level outputted from the sensor is above the predefined threshold. The threshold value should be provided by the manufacturer but it can also be determined experimentally.

4.2.2 MAGNETOMETER

In Phase B documentation [PW-Sat2-B-01.00-ADCS-PDR], placing one additional magnetometer on the satellite, especially for the detumbling mode was considered. It was motivated by the couple of arguments. First of all, the magnetometer could be placed in a place where the magnetic interference from other satellite components is minimal. Additionally, the developed ADCS system would be autonomous, e.g. with respect to chosen actuators (for example if reaction wheels are used in the future). However, in the satellite design there is already one magnetometer available on the magnetorquers board supplied by ISIS. It is a XEN1210 magnetometer with flight heritage. In order to simplify the design and maximise the reliability of the system, this magnetometer will be used for magnetic field vector indication in the detumbling mode. No additional magnetometers will be placed in the satellite.

Table 4-3 shows the specification of the internal single axis XEN1210 magnetometer [5] placed on magnetorquers board.

Table 4-3 XEN1210 Magnetometer Specification

Parameter	Value
Field range	±63 mT
Noise	55 nT/√Hz
Hysteresis	10 nT
Supply voltage (typ.)	3.3 V
Resolution (24 bits)	7.5 nT/LSB
Operating temperature range	-40 to +125 °C

4.2.3 GYROSCOPES

When choosing the gyroscope, noise, sensitivity, bias instability and temperature sensitivity are critical performance parameters. Gyroscopes are used primarily in two situations. Firstly, to monitor the performance of the detumbling algorithm and in order to determine the moment when detumbling mode can be turned off. Secondly, in the sun point mode in sensor fusion to estimate the attitude to the Sun and angular rate of the satellite. What is more, with the use of gyroscope the satellites behaviour during different mission phases (e.g.

	PW-Sat2	Critical Design Review	
	2016-11-30		
	Phase C	Attitude Determination and Control System	

sail deployment) can be investigated. In the phase B documentation, the Analog Devices' ADXRS453 yaw-axis gyroscope was chosen for the PW-Sat2 satellite. However, the choice was reconsidered. ADCSRS453 present very good characteristics and has a significant flight heritage. On the other hand, using this gyroscope would require an additional mechanical structure so that the angular rate could be measured in all three axes of the satellite since single gyroscope indicates angular rate only in one axis. Moreover, from the point of view of the OBC team, an I2C interface for communication with gyroscopes is desired. Additional research on the gyroscopes selection was performed in order to investigate if the ADCSRS453 gyroscope could be replaced with a three axis gyroscope equipped with an I2C interface. The research lead to four possible replacements: MPU3300, A3G4250D, ITG-3200, L3G4200D. Finally the InvenSense ITG-3200 3-axis gyroscope was chosen. The choice was made mainly due to the specification, availability and flight heritage of that sensor. Table 4-7 shows the specification of the ITG-3200 gyroscope.

Table 4-4 ITG-3200 Gyroscope Specification

Parameter	Value	Comment
Measurement range	$\pm 2000 \text{ } ^\circ/\text{s}$	-
Sensitivity Scale Factor	14.375 LSB/ $^\circ/\text{s}$	-
Sensitivity Scale Factor Variation Over Temperature	$\pm 10\%$	-
Total RMS noise	0.38 $^\circ/\text{s-rms}$	100Hz LPF
Cross-axis Sensitivity	2%	-
Nonlinearity	0.2%	Best fit straight line; 25°C
Supply voltage	2.1 V	min
	3.6 V	max
Communication interface	I2C	-
Operating temperature range	-40 to +85 °C	-

4.3 CONCLUSIONS

The team has investigated many sensors configurations to use. In the selection phase the focus on simplicity, reliability and performance was made. It was possible to simplify the ADCS system in such a way that the accuracy and performance is kept at the sufficient level, based on the simulation analysis. Still electrical, thermal, mechanical and other environmental characteristics will have to be investigated in detail in order to assure interface compatibility with the other satellite's subsystems.

	PW-Sat2	Critical Design Review	
	2016-11-30		
	Phase C	Attitude Determination and Control System	

5 ADCS ARCHITECTURE

The control strategy for sun pointing mode has changed since documentation Phase B. With 3 magnetorquers, the team has not developed the algorithm to maintain constant satellite's attitude in ECI inertial frame with the presence of the external torque. Since nadir pointing is not considered after the mission plan review, the major task of the ADCS is Sun pointing. The team has decided to utilize the gyroscopic effect and stabilize the axis of rotation in ECI inertial frame. With these requirements, ADCS is necessary to maintain constant angular rate around satellite's +X axis equal approximately to $5^{\circ}/s$. Using this novel approach, pointing solar panels towards the Sun can be made possible, assuming that Sun vector is collinear with the satellite's +X axis perpendicular to deployed solar panels' plane. Further details on the Sun Pointing controller are presented in chapter 7.3.1.

In the figure below, the ADCS block diagram is presented. It is related to Sun Pointing mode, when the attitude determination and estimation algorithms are utilized. Thus information from Sun Sensor, magnetometer and gyroscope is necessary. In detumbling mode, with B-Dot algorithm, only magnetometer data is used and no attitude determination and estimation is performed, making the ADCS algorithm relatively simple.

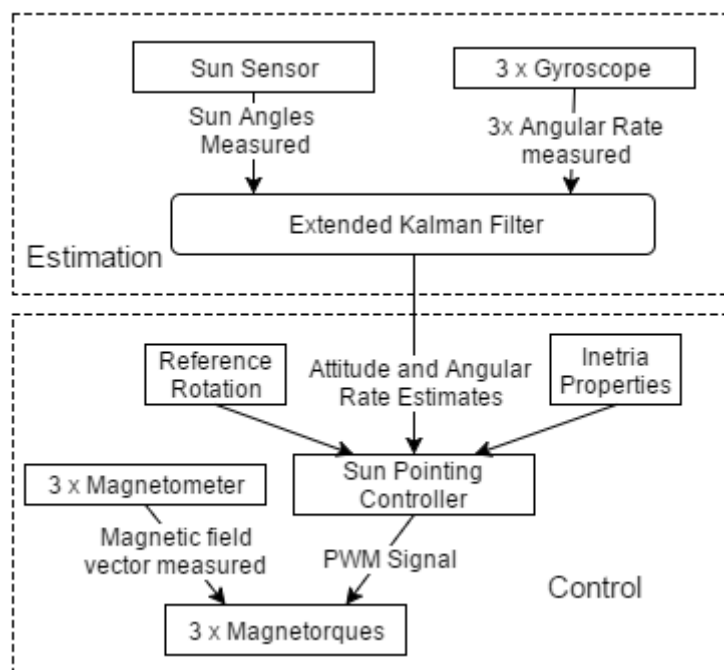


Figure 5-1 ADCS Block Diagram for Sun Pointing Mode

In following subsections, an overview of attitude and angular rate determination and control strategy is presented. Required algorithms and environmental models are described briefly. Detailed discussion on attitude

	PW-Sat2	Critical Design Review	
	2016-11-30		
	Phase C	Attitude Determination and Control System	

and angular rate determination and estimation, as well as control algorithms is presented in sections 5.1 and 6.2, respectively.

5.1 DETERMINATION

Attitude and angular rate determination and estimation algorithms are necessary only in Sun Pointing mode. Brief description of each algorithm and environmental models are presented below.

Extended Kalman Filter

The attitude determination problem is nonlinear, therefore Extended Kalman Filter has to be used. EKF provides estimate of the noisy data and its output is more accurate than obtained from deterministic, static attitude determination methods, for example TRIAD. Moreover, EKF provides information about the attitude in eclipse, when the Sun Sensor measurement is not available. Nevertheless, it has to be initialized with at least two observations outside eclipse.

5.2 CONTROL

In this chapter brief description of Sun Pointing and B-dot algorithm is presented. Further details can be found in chapter 6.2.

Sun Pointing

Sun Pointing mode requires spinning the satellite about satellite's +X axis and pointing it towards the Sun. Spin stabilization keeps the Sun tracking error in predetermined limits. The control law is based on the desired angular momentum, precession and nutation error. The control law requires therefore information about inertia matrix, current angular rate and attitude of the satellite with reference to ECI inertial frame.

B-Dot

B-Dot algorithm is the simplest one for detumbling. It is widely used to decelerate angular rotation after P-POD deployment. It needs information of Earth's magnetic field changes in satellite's frame. Therefore, two subsequent magnetometer measurements are required. The basic assumption is that the changes of magnetic field measurements in body frame are due to the satellite's rotational movement. Stability of the B-Dot control law is proven with Lyapunov's second method for stability. High-pass filter is utilized in order to filter data when calculating the discrete derivative based on noisy data. Built-in autonomous detumbling mode on iMTQ board activates when the predetermined threshold of the angular rate is exceeded.

5.3 ADCS MODES

As mentioned in chapter 2, the number of ADCS modes were minimized after mission plan review. Also, the simplicity of the ADCS is one of the dominant requirements, thus making the transitions between modes less complex had to be considered. In this chapter, 4 ADCS modes are presented.

	PW-Sat2	Critical Design Review	
	2016-11-30		
	Phase C	Attitude Determination and Control System	

- SAFE/OFF

In this mode, the ADCS is not working. Sensors' and actuators' power supply is cut off. ADCS will be in SAFE/OFF mode in initial phase of the mission. Also, transition to this mode has to be done autonomously when battery level drops below some predetermined threshold or after sending telecommand when data obtained from telemetry will denote the ADCS malfunction.

- DETUMBLING

This mode activates after first turn on of the power supply in the initial phase of the mission. Autonomous transition to this mode has to be done after exceeding predetermined threshold of the angular rate. DETUMBLING mode requires magnetometer and at least two actuators working properly.

- STANDBY

In this mode, the attitude is estimated based on sensors' data, but no attitude control is performed. Transition to this mode is possible after DETUMBLING mode or actuators' malfunction. Then, estimating the attitude is necessary to compare the data with experimental Sun Sensor's data and to check the overall performance of the attitude determination and estimation algorithms.

- SUN POINTING

This mode is activated after detumbling in initial phase of the mission, providing that solar panels are deployed. Transition to this mode is possible from STANDBY mode, after assuring EKF convergence, because controlling the attitude based on not filtered sensors data consumes much more energy. SUN POINTING mode requires all sensors and at least two actuators working properly.

In the table below, the timeline of the ADCS is presented. Nominal ADCS mode is Sun Pointing with rotation 5°/s about the satellite's X axis.

Table 5-1 ADCS on-orbit sequence

No.	Event
1.	PW-Sat2 is deployed from P-POD, power is on, start ADCS system
2.	Start Detumbling mode
3.	When satellite's angular rate reached predetermined threshold, finish Detumbling
4.	Receive TLE orbital and time data from ground
5.	Start Standby mode
6.	When deployment of solar panels confirmed, start nominal Sun Pointing mode

	PW-Sat2	Critical Design Review	
	2016-11-30		
	Phase C	Attitude Determination and Control System	

6 DESIGN ANALYSIS

6.1 EXTENDED KALMAN FILTER

The Multiplicative Extended Kalman Filter (MEKF) adopted in PDR has been considerably simplified, which justification is as follows. In the Sun Pointing control mode, the spin controller requires the information of the Sun vector and satellite's angular rate in the body frame. This information is required to control the satellite's spin direction and magnitude. The Sun vector in the body frame can be obtained in two ways, either directly from the Sun sensor angle measurements or by estimating the satellite's attitude in the ECI frame and transforming the Sun vector in the ECI frame to the body frame. The second method is more elaborate as it requires satellite's quaternion estimation and storing the Sun position model onboard. Furthermore, to estimate the satellite's quaternion with a satisfactory accuracy, additional sensors data processing is necessary, e.g. from a magnetometer. This in turn requires storing elaborate IGRF model and orbit propagator onboard. For these reasons, the simplified version of the EKF is adopted which uses the measurements only from the Sun sensor and the gyroscope. Note that this architecture is possible due to the presence of relatively accurate Sun sensor. Below, the implications of this design decision are stated:

- The magnetometer is not used for navigation purposes, hence the reference IGRF model is not necessary. This, in turn, makes the satellite's position calculation in the ECI frame obsolete. Therefore, the IGRF and SGP4 models are not necessary.
- The Sun sensor angle measurement are processed directly and the navigation filter design concept is not based on comparing the Sun sensor measurement with the Sun vector in the ECI frame. Also, as previously stated, the Sun vector in the ECI frame is no longer used in the control law. Therefore, the Sun position model in the ECI frame is not necessary.
- Since the orbit propagator model is not used onboard, sending the TLE data to update the position estimates is not necessary. This makes the ADCS more robust to the problems with Earth-satellite communication. Problems with CubeSats communication modules jeopardized past mission frequently, which is known in the community. In fact, this was the primary motivation to change the ADCS algorithms design so that they do not rely on the TLE updates. The team carried out the analysis which revealed that the J2 and SGP4 orbit propagators estimate the satellite's position with a sufficient accuracy up to 7 and 9 days, for the J2 and SGP4, respectively. Considering the mission time duration, this is not acceptable. Since the GPS receiver was discarded due to the cost, mass and volume constraints, the decision was made not to rely the ADCS algorithms on the satellite's position in the ECI frame.
- In the PDR, the satellite's position in the ECI frame was used to determine whether the satellite is in eclipse or not. This information was used to suspend the attitude control in eclipse, namely to turn the magnetorquers off. With the orbit propagator onboard not present anymore, this condition can no longer

	PW-Sat2	Critical Design Review	
	2016-11-30		
	Phase C	Attitude Determination and Control System	

be determined using the satellite's position. Hence, the Sun Presence flag is defined on the basis of the voltage threshold, which enables to determine whether the Sun is in the FoV of the Sun sensor. Furthermore, it was decided to suspend the attitude control when the Sun Presence flag is false, which results in SS validity flag set to false. Note that no explicit eclipse flag is therefore used.

In the following sections, the states, the measurements and corresponding equations of the estimator are presented.

6.1.1 ARCHITECTURE

The measurement vector, \mathbf{z} , consists of two Sun sensor angle measurements, namely the latitude, θ , and longitude, λ , and the satellite's angular rate in body frame, $\boldsymbol{\omega}$. The latitude is the angle between the Sun unit vector and the Sun sensor frame's +Z axis. The longitude is defined as the angle between the Sun vector's projection on the Sun sensor XY plane and the Sun sensor frame's +X axis direction. The positive sign of the longitude is towards the +Y axis direction. The state vector, \mathbf{x} , consists of the same elements as the measurement vector, which gives:

$$\mathbf{x} = \mathbf{z} = \begin{bmatrix} \theta \\ \lambda \\ \boldsymbol{\omega} \end{bmatrix} \quad (6.1)$$

Two Sun sensor angle measurements are consistent with the sensor output form. They uniquely define the Sun vector in the Sun sensor frame, \mathbf{s}_s :

$$\mathbf{s}_s = \begin{bmatrix} \sin\theta \cos\lambda \\ \sin\theta \sin\lambda \\ \cos\theta \end{bmatrix} \quad (6.2)$$

The inverse transformation is given by:

$$\theta = \arccos(s_z) \quad (6.3a)$$

$$\lambda = 2\arctan\left(\frac{s_y}{\sqrt{1-s_z^2+s_x^2}}\right) \quad (6.3b)$$

where the Eq. 6.3b includes the correct quadrant, and hence $\lambda \in (-\pi, \pi)$. Equation 6.3b is obtained by using the following relationship:

$$\tan\left(\frac{\lambda}{2}\right) = \frac{\sin\lambda}{1+\cos\lambda}$$

After simple manipulations and substituting Sun vector components along X and Y axis from Eq. 6.2, the equation 6.3b is obtained. Note that the Sun vector in the body frame can be calculated by transforming the Sun vector components in the Sun sensor frame to the body frame:

$$\mathbf{s}_b = \mathbf{A}_s^T \mathbf{s}_s \quad (6.4)$$

	PW-Sat2	Critical Design Review	
	2016-11-30		
	Phase C	Attitude Determination and Control System	

where the attitude matrix \mathbf{A}_s denotes the orientation of the Sun sensor frame with respect to the body frame. In the subsequent sections, the components of the Sun vector refers to the components expressed in Sun sensor frame, hence the subscript s is omitted for brevity.

6.1.1.1 Propagation

Given the previous state vector estimate, \mathbf{x}_{k-1}^+ , the state is propagated through the dynamics equations to obtain the predicted, *a priori*, state in the current iteration, \mathbf{x}_k^- . The continuous state dynamics model is given by:

$$\dot{\mathbf{x}} = \mathbf{f}(\mathbf{x}, \mathbf{u}) = \begin{bmatrix} \dot{\theta} \\ \dot{\lambda} \\ \dot{\omega} \end{bmatrix} \quad (6.5)$$

where the input vector is denoted by \mathbf{u} . The Sun sensor angles time derivatives are calculated using the chain rule:

$$\dot{\theta} = \frac{d\theta}{ds_s} \frac{ds_s}{ds_b} \frac{ds_b}{dt} \quad (6.6a)$$

$$\dot{\lambda} = \frac{d\lambda}{ds_s} \frac{ds_s}{ds_b} \frac{ds_b}{dt} \quad (6.6b)$$

where the derivatives of the Sun angles with respect to the Sun vector given in the Sun sensor frame are given by:

$$\frac{d\theta}{ds_s} = \begin{bmatrix} \frac{d\theta}{ds_x} & \frac{d\theta}{ds_y} & \frac{d\theta}{ds_z} \end{bmatrix} = \begin{bmatrix} 0 & 0 & \frac{-1}{\sqrt{1-s_z^2}} \end{bmatrix} \quad (6.7a)$$

$$\frac{d\lambda}{ds_s} = \begin{bmatrix} \frac{d\lambda}{ds_x} & \frac{d\lambda}{ds_y} & \frac{d\lambda}{ds_z} \end{bmatrix} = \frac{2}{(s^2+1)\left(\sqrt{1-s_z^2+s_x}\right)} \begin{bmatrix} -\frac{s_y}{\sqrt{1-s_z^2+s_x}} & 1 & \frac{s_y s_z}{\left(\sqrt{1-s_z^2+s_x}\right)\sqrt{1-s_z^2}} \end{bmatrix} \quad (6.7b)$$

Note that there is a singularity for $\theta = 0$, which result in $s_z = 1$ and $s_x = s_y = 0$. This corresponds to the Sun vector being directly above the Sun sensor head. If the Sun sensor would be mounted on the satellite's +X face such that in the nominal configuration, the Sun would be directly along the Sun sensor +Z axis, this would lead to numerical problems and hence greater errors. Therefore, the Sun sensor's normal is rotated by 25° with respect to the satellite's +X axis. Assuming no pointing errors, in the nominal configuration, the latitude angle measurement is equal to 25° . The following rotation matrix describes the Sun sensor frame orientation with respect to the satellite's body frame:

$$\mathbf{A}_s = \begin{bmatrix} 1 & 0 & 0 \\ 0 & \cos(25^\circ) & \sin(25^\circ) \\ 0 & -\sin(25^\circ) & \cos(25^\circ) \end{bmatrix} \begin{bmatrix} 0 & 0 & -1 \\ 0 & 1 & 0 \\ 1 & 0 & 0 \end{bmatrix} = \begin{bmatrix} 0 & 0 & -1 \\ \sin(25^\circ) & \cos(25^\circ) & 0 \\ \cos(25^\circ) & -\sin(25^\circ) & 0 \end{bmatrix}$$

where the first rotation is performed around the +Y axis by 90° , so that the Sun sensor frame +Z axis is aligned with the satellite's +X frame. The second rotation is performed around the new Sun sensor frame +X axis by 25° . The chosen value of 25° represents a trade-off between the SS FoV and expected pointing accuracy.

The $\frac{ds_s}{ds_b}$ term in Eqs. 6.6 is simply given by \mathbf{A}_s , see Eq. 6.4.

	PW-Sat2	Critical Design Review	
	2016-11-30		
	Phase C	Attitude Determination and Control System	

The time derivative of the Sun vector in body frame can be obtained as follows. The Sun vector in body frame is related to the Sun vector in the ECI frame using the satellite's orientation in the ECI frame, \mathbf{A} :

$$\mathbf{s}_b = \mathbf{A}\mathbf{s}_i \quad (6.8)$$

Differentiating the above equation with respect to time, yields:

$$\dot{\mathbf{s}}_b = \dot{\mathbf{A}}\mathbf{s}_i + \mathbf{A}\dot{\mathbf{s}}_i \approx \dot{\mathbf{A}}\mathbf{s}_i \quad (6.9)$$

where it is assumed, that the Sun vector in the ECI frame is constant for a given iteration time. The time derivative of the attitude matrix is given by:

$$\dot{\mathbf{A}} = -[\boldsymbol{\omega} \times] \mathbf{A} \quad (6.10)$$

where the satellite's angular rate is expressed in the body frame. Substituting Eq. 6.10 to Eq. 6.9 gives:

$$\dot{\mathbf{s}}_b = -[\boldsymbol{\omega} \times] \mathbf{s}_b \quad (6.11)$$

Substituting above results to the Eqs. 6.6 yields:

$$\dot{\theta} = -\frac{d\theta}{ds_s} \mathbf{A}_s [\boldsymbol{\omega} \times] \mathbf{A}_s^T \mathbf{s}_s \quad (6.12a)$$

$$\dot{\lambda} = -\frac{d\lambda}{ds_s} \mathbf{A}_s [\boldsymbol{\omega} \times] \mathbf{A}_s^T \mathbf{s}_s \quad (6.12b)$$

where the Eq. 6.4 has been used. Note that the term $\mathbf{A}_s [\boldsymbol{\omega} \times] \mathbf{A}_s^T$ is the skew-symmetric matrix of the satellite's angular rate expressed in the Sun sensor frame, $\boldsymbol{\omega}_s$:

$$[\boldsymbol{\omega}_s \times] = \mathbf{A}_s [\boldsymbol{\omega} \times] \mathbf{A}_s^T \mathbf{s}_s$$

Substituting this to the Eq. 6.12 gives:

$$\dot{\theta} = -\frac{d\theta}{ds_s} [\boldsymbol{\omega}_s \times] \mathbf{s}_s \quad (6.13a)$$

$$\dot{\lambda} = -\frac{d\lambda}{ds_s} [\boldsymbol{\omega}_s \times] \mathbf{s}_s \quad (6.13b)$$

The angular rate dynamics is given by the Euler equation:

$$\dot{\boldsymbol{\omega}} = \mathbf{I}^{-1} \{ \mathbf{T}_{ctrl} - [\boldsymbol{\omega} \times] (\mathbf{I} \cdot \boldsymbol{\omega}) \} \quad (6.14)$$

where the control torque is the control torque from the previous time step.

Equations 6.13 and 6.14 are integrated in time using the Runge-Kutta 4th order method and the *a priori* state estimates are obtained. Note that the time derivatives are calculated for the previous state estimate, \mathbf{x}_{k-1}^+ .

The state covariance at previous time step, \mathbf{P}_{k-1}^+ , is propagated through the discrete equation to obtain the *a priori* state covariance at the current time step, \mathbf{P}_k^- :

$$\mathbf{P}_k^- = \Phi_{k-1} \mathbf{P}_{k-1}^+ \Phi_{k-1}^T + \Delta t \cdot \mathbf{Q} \quad (6.15)$$

where \mathbf{Q} denotes the state dynamics covariance, and Φ_{k-1} is a discrete process Jacobian given by:

	PW-Sat2	Critical Design Review	
	2016-11-30		
	Phase C	Attitude Determination and Control System	

$$\Phi = e^{\mathbf{F}\Delta t} \approx \mathbf{1} + \mathbf{F}\Delta t \quad (6.16)$$

where the above approximation is valid for small time steps. The matrix \mathbf{F} is a continuous process Jacobian consisting of the following partial derivatives calculated for the previous time step:

$$\mathbf{F} = \left. \frac{\partial \mathbf{f}}{\partial \mathbf{x}} \right|_{\mathbf{x}=\mathbf{x}_{k-1}^+} \quad (6.17)$$

The computation of the Sun sensor measurement angles derivatives will be presented on the basis of the latitude angle. Differentiating Eq. 6.12a with respect to the state vector variables, gives:

$$\frac{\partial \dot{\theta}}{\partial \theta} = -\frac{\partial}{\partial \theta} \left(\frac{d\theta}{ds_s} \right) \mathbf{A}_s [\boldsymbol{\omega} \times] \mathbf{A}_s^T \mathbf{s}_s - \frac{d\theta}{ds_s} \mathbf{A}_s [\boldsymbol{\omega} \times] \mathbf{A}_s^T \frac{ds_s}{d\theta} \quad (6.18a)$$

$$\frac{\partial \dot{\theta}}{\partial \lambda} = -\frac{\partial}{\partial \lambda} \left(\frac{d\theta}{ds_s} \right) \mathbf{A}_s [\boldsymbol{\omega} \times] \mathbf{A}_s^T \mathbf{s}_s - \frac{d\theta}{ds_s} \mathbf{A}_s [\boldsymbol{\omega} \times] \mathbf{A}_s^T \frac{ds_s}{d\lambda} \quad (6.18b)$$

$$\frac{\partial \dot{\theta}}{\partial \boldsymbol{\omega}} = \frac{d\theta}{ds_s} \mathbf{A}_s [(\mathbf{A}_s^T \mathbf{s}_s) \times] \quad (6.18c)$$

First, the derivatives of the Sun vector in the Sun sensor frame with respect to the latitude and longitude angles are calculated:

$$\frac{ds_s}{d\theta} = \begin{bmatrix} \cos\theta \cos\lambda \\ \cos\theta \sin\lambda \\ -\sin\theta \end{bmatrix} \quad (6.19a)$$

$$\frac{ds_s}{d\lambda} = \begin{bmatrix} -\sin\theta \sin\lambda \\ \sin\theta \cos\lambda \\ 0 \end{bmatrix} \quad (6.19b)$$

In order to differentiate Eq. 6.7 with respect to the Sun angles, it is convenient to express the Sun vector components in terms of the Sun angles, which gives:

$$\frac{d\theta}{ds_s} = \begin{bmatrix} 0 & 0 & -\frac{1}{\sin\theta} \end{bmatrix} \quad (6.20a)$$

$$\frac{d\lambda}{ds_s} = \begin{bmatrix} -\frac{\tan(\frac{\lambda}{2})}{\sin\theta} & \frac{1}{\sin\theta} & \frac{\cos\theta \tan(\frac{\lambda}{2})}{\sin^2\theta} \end{bmatrix} \quad (6.20b)$$

Four partial derivatives are given below:

$$\frac{\partial}{\partial \theta} \left(\frac{d\theta}{ds_s} \right) = \begin{bmatrix} 0 & 0 & \frac{\cos\theta}{\sin^2\theta} \end{bmatrix} \quad (6.21a)$$

$$\frac{\partial}{\partial \lambda} \left(\frac{d\theta}{ds_s} \right) = [0 \ 0 \ 0] \quad (6.21b)$$

$$\frac{\partial}{\partial \theta} \left(\frac{d\lambda}{ds_s} \right) = \begin{bmatrix} \frac{\cos\theta}{\sin^2\theta} \tan\frac{\lambda}{2} & \frac{-\cos\theta}{\sin^2\theta} & \frac{-\tan^2\frac{\lambda}{2}}{\sin\theta} \left(\frac{2}{\sin^2\theta} - 1 \right) \end{bmatrix} \quad (6.21c)$$

$$\frac{\partial}{\partial \lambda} \left(\frac{d\lambda}{ds_s} \right) = \begin{bmatrix} \frac{-1}{2\sin\theta} \left(1 + \tan^2\frac{\lambda}{2} \right) & 0 & \frac{\cos\theta}{2\sin^2\theta} \left(1 + \tan^2\frac{\lambda}{2} \right) \end{bmatrix} \quad (6.21d)$$

Note that the longitude angle partial derivatives, i.e. $\frac{\partial \lambda}{\partial \theta}$, $\frac{\partial \lambda}{\partial \lambda}$ and $\frac{\partial \lambda}{\partial \boldsymbol{\omega}}$ are calculated analogously to the Eq. 6.18.

	PW-Sat2	Critical Design Review	
	2016-11-30		
	Phase C	Attitude Determination and Control System	

The angular rate dynamics, given by Eq. 6.14 does not depend on the Sun angles explicitly, hence:

$$\frac{d\dot{\omega}}{d\theta} = \frac{d\dot{\omega}}{d\lambda} = \begin{bmatrix} 0 \\ 0 \\ 0 \end{bmatrix} \quad (6.22)$$

The angular rate time derivative differentiated with respect to the angular rate itself, yields:

$$\frac{d\ddot{\omega}}{d\omega} = \mathbf{I}^{-1}\{[\mathbf{I} \cdot \boldsymbol{\omega} \times] - [\boldsymbol{\omega} \times] \mathbf{I}\} \quad (6.23)$$

Substituting above results to the Eq. 6.17 yields the following continuous Jacobian matrix:

$$\mathbf{F} = \begin{bmatrix} \frac{\partial \dot{\theta}}{\partial \theta} & \frac{\partial \dot{\theta}}{\partial \lambda} & \frac{\partial \dot{\theta}}{\partial \omega} \\ \frac{\partial \dot{\lambda}}{\partial \theta} & \frac{\partial \dot{\lambda}}{\partial \lambda} & \frac{\partial \dot{\lambda}}{\partial \omega} \\ \mathbf{0}_{3 \times 1} & \mathbf{0}_{3 \times 1} & \frac{d\ddot{\omega}}{d\omega} \end{bmatrix} \quad (6.24)$$

Substituting continuous state dynamics Jacobian to the Eq. 6.16 and then 6.15 yields the *a priori* state covariance matrix, \mathbf{P}_k^- .

6.1.1.2 Update

Since the state and measurement vectors are equal, the observation matrix, \mathbf{H} , defined as, $\mathbf{z} = \mathbf{Hx}$, is simply given by an identity matrix, $\mathbf{H} = \mathbf{1}_{5 \times 5}$. Therefore, the predicted measurement at time step k , \mathbf{z}_k^- , is equal to the *a priori* state vector, \mathbf{x}_k^- :

$$\mathbf{z}_k^- = \mathbf{x}_k^- \quad (6.25)$$

Innovation (or residual) covariance, \mathbf{S} , is given by:

$$\mathbf{S} = \mathbf{H}\mathbf{P}_k^-\mathbf{H}^T + \mathbf{R} \quad (6.26)$$

where \mathbf{R} matrix denotes the measurement covariance, thus corresponds to the sensors noise variance. The Kalman gain matrix is calculated as follows:

$$\mathbf{K} = \mathbf{P}_k^-\mathbf{H}^T\mathbf{S}^{-1} \quad (6.27)$$

Finally, the *a posteriori* state vector is given by:

$$\mathbf{x}_k^+ = \mathbf{x}_k^- + \mathbf{K}(\mathbf{z}_k - \mathbf{z}_k^-) \quad (6.28)$$

where the measurement vector, \mathbf{z}_k , corresponds to the Sun angles measurements and gyro measurement at the current time step:

$$\mathbf{z}_k = \begin{bmatrix} \theta_k \\ \lambda_k \\ \boldsymbol{\omega}_k \end{bmatrix} \quad (6.29)$$

	PW-Sat2	Critical Design Review	
	2016-11-30		
	Phase C	Attitude Determination and Control System	

The *a posteriori* state covariance matrix is calculated using the so-called Joseph form which is more numerically stable, as it ensures that the state covariance matrix is positive-definite:

$$\mathbf{P}_k^+ = (\mathbf{1}_{5 \times 5} - \mathbf{K}\mathbf{H})\mathbf{P}_k^- (\mathbf{1}_{5 \times 5} - \mathbf{K}\mathbf{H})^T + \mathbf{K}\mathbf{R}\mathbf{K}^T \quad (6.30)$$

Based on the set of simulations and sensors errors specification, the process', measurement and initial state covariance matrices are set to:

$$\mathbf{Q} = \text{diag}(1 \ 1 \ 1 \ 10 \ 10 \ 10) 10^{-8}$$

$$\mathbf{R} = \text{diag} \left[\left(0.5 \cdot \frac{\pi}{180} \right)^2 \ \left(0.5 \cdot \frac{\pi}{180} \right)^2 \ \left(0.3 \cdot \frac{\pi}{180} \right)^2 \ \left(0.3 \cdot \frac{\pi}{180} \right)^2 \ \left(0.3 \cdot \frac{\pi}{180} \right)^2 \right]$$

$$\mathbf{P}_0 = \text{diag} \left[\left(3 \cdot 0.5 \cdot \frac{\pi}{180} \right)^2 \ \left(3 \cdot 0.5 \cdot \frac{\pi}{180} \right)^2 \ \left(0.3 \cdot \frac{\pi}{180} \right)^2 \ \left(0.3 \cdot \frac{\pi}{180} \right)^2 \ \left(0.3 \cdot \frac{\pi}{180} \right)^2 \right]$$

6.1.1.3 Initialization Logic

The filter must be initialized outside eclipse, when both measurements from the Sun sensor and the gyro are valid AND the filter initialization flag is set to true. The initial state estimates are set to the current measurements, namely $\mathbf{x}_0^+ = \mathbf{z}_0$ and the state covariance is set to $\mathbf{P}_0^+ = \mathbf{P}_0$. These values, i.e. \mathbf{x}_0^+ and \mathbf{P}_0^+ , serve as the state and covariance estimates at the 'previous' time step for the next iteration, $k = 1$.

Note that due to the SS FoV it can happen that the satellite is outside the eclipse, but due to the unfavorable attitude, the Sun is not within the SS FoV. The ADCS then waits until the Sun is within the SS FoV. It was found that there is 99.9% probability that the Sun will be in the SS FoV within the 5 orbits. This result was obtained assuming random initial attitude and the angular rates corresponding to the final angular rates after detumbling. No attitude control has been included, but the disturbance torques have been added.

Therefore, when the filter initialization flag is set to true, the ADCS waits for the valid SS and gyro measurements. Once it is initialized, the initialization flag is set to false. First Sun Pointing initialization will be pre-programmed, hence for the given time, dependent on the mission scenario, the filter initialization flag will be set to true. Once the filter is initialized, it can be re-initialized after the TC is sent to set the filter initialization flag to true. Therefore, no autonomous re-initialization is incorporated.

It is best to set the initial state estimate equal to the measurements, since the expected error of the initial estimate is relatively low and corresponds to the accuracy of the sensors. Note that some predefined, fixed values could be chosen, but it may result in large Sun angle and angular rate errors. For the Sun angles it could yield the attitude error estimates up to 180°, which would require more time for the filter to converge. For these reasons, it is decided to set the initial state vector equal the measurements.

6.1.1.4 Sensors Outage Handling

If the sensor validity flag is false, then no update corresponding to the given sensor's information is performed. To accommodate the common structure of the filter, the corresponding measurement is hardcoded to be equal to

	PW-Sat2	Critical Design Review	
	2016-11-30		
	Phase C	Attitude Determination and Control System	

the predicted measurement, so that the corresponding innovation is equal 0. To include the sensors outage in the residual covariance matrix, the corresponding columns of the Kalman gain matrix, shall be set to 0 as well. This is presented in

Table 6-1.

Table 6-1 Sensors Outage Handling

Sensor Flag	Innovation	Kalman Gain
Sun Sensor Validity Flag = false	$\theta_k = \theta_k^-$ $\lambda_k = \lambda_k^-$	$\mathbf{K}(:, [1,2]) = \mathbf{0}_{5 \times 2}$
Gyroscope Validity Flag = false	$\omega_k = \omega_k^-$	$\mathbf{K}(:, [3,4,5]) = \mathbf{0}_{5 \times 3}$

The ‘:’ notation in Kalman gain column denotes all rows, and the ‘[1,2]’ notation refers to the first and second columns.

6.1.1.5 Filter Convergence

The filter convergence flag is set to true when enough valid sensor measurements have been processed. For the Sun sensor and the gyro, the counter logic is implemented separately. When a valid measurement is processed, the counter is incremented by +1 and the invalid measurement is received, the counter increments by -1. Both Sun sensor and gyro counters starts at 0. The filter convergence flag is set to true when the Sun sensor AND the gyro counters reach their converge thresholds, α_{ss} and α_{gyr} , respectively.

When the convergence thresholds are reached, the counter continues to operate, until β_{ss} and β_{gyr} are reached, such that $\beta_{ss} > \alpha_{ss}$ and $\beta_{gyr} > \alpha_{gyr}$. This ensures that when the filter has converged and the invalid sensor measurement is received, the filter convergence flag is not set to false immediately.

After the counter reaches β , and the valid measurement is received, the counter value continues to be equal β . Also, when the counter is set to 0 (either due to the initialization or after processing many invalid measurements) and the invalid measurement is received, the counter value continues to be equal 0. Therefore, for the give sensor counter, its value can only be in the range $(0, \beta)$.

The values of α_{ss} , α_{gyr} , β_{ss} and β_{gyr} have not been chosen yet. They will be defined on the basis of the sensors and the EKF performance. The EKF performance will be assessed using the Monte Carlo simulations.

6.1.1.6 Attitude Control Suspension

It has been decided that the signal is sent to the actuators when the filter convergence flag AND both the sensors validity flags are true. Therefore, the iMTQ are not commanded when the filter has converged, but either sensor's flag is false. This adds robustness for the unmodeled system dynamics. Note that when the control commanding would be based only on the filter convergence flag, then the actuators would be engaged when the filter acts as a propagator. This corresponds to the situation when the either sensor validity flag is false, but the

	PW-Sat2	Critical Design Review	
	2016-11-30		
	Phase C	Attitude Determination and Control System	

counter in the filter convergence logic has not reached the threshold yet, hence the filter convergence flag is still set to true. More trust is put into the sensors data, hence the requirement for the both sensors validity flags to be true, when the controller is turned on.

This functionality also ensures commonality for the filter initialization, eclipse and some infrequent invalid sensors measurements cases.

For the initialization case, the filter must process enough valid sensors measurements to set the filter convergence flag to true. Also, current sensors measurements must be valid in order to send the signal to the actuators.

For the eclipse case, the actuators are turned off immediately after entering the eclipse, due to the Sun Sensor validity flag set to false. Therefore, the ADCS does not wait until the filter convergence flag is set to false. After leaving the eclipse, the ADCS waits until the filter convergence flag is set to true and then engages the controller.

Some infrequent/single sensor data outage causes the iMTQ to be turned off. It does not affect the controller performance significantly, but allows to share the commonality with the eclipse case.

6.2 ATTITUDE CONTROL

The only actuators used for attitude control in PW-Sat2 are the magnetorquers. Two control modes are implemented, namely the detumbling and the Sun Pointing, which are further discussed in the subsequent sections.

6.2.1 MAGNETORQUERS

The iMTQ board consists of 3 perpendicular electromagnetic coils, one along each satellite's body axis. When current is applied to each perpendicular coil, the 3 dimensional magnetic dipole is generated in space. When magnetic dipole \mathbf{m}_{ctrl} is in magnetic field \mathbf{B} , the torque is generated according to Eq. 6.31:

$$\mathbf{T}_{ctrl} = \mathbf{m}_{ctrl} \times \mathbf{B} \quad (6.31)$$

where all vectors are expressed in satellite's body frame and subscript *ctrl* denotes control.

Only the component of the commanded torque perpendicular to the Earth's magnetic field vector will be generated. This is presented in the figure below.

	PW-Sat2	Critical Design Review	
	2016-11-30		
	Phase C	Attitude Determination and Control System	

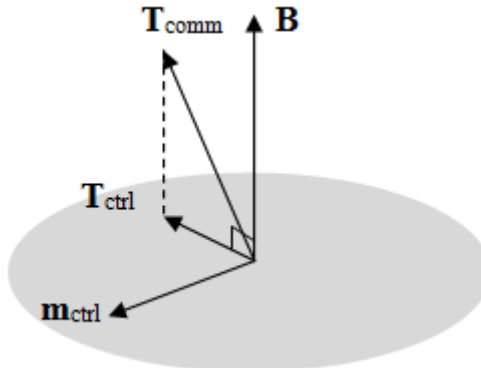


Figure 6-1 Underactuation of the magnetic control system

Given the commanded control torque \mathbf{T}_{comm} and Earth's magnetic field \mathbf{B} , the dipole \mathbf{m}_{ctrl} which has to be generated in order to create control torque \mathbf{T}_{ctrl} , can be derived on the basis of Figure 6-1:

$$\mathbf{m}_{\text{ctrl}} = \frac{\mathbf{B} \times \mathbf{T}_{\text{comm}}}{\|\mathbf{B}\|^2} \quad (6.32)$$

The magnetic field in the satellite body frame, \mathbf{B} , is read directly from the magnetometer. The iMTQ accepts the commanded magnetic dipole as an input and applies the PWM signal with the appropriate duty cycle to the coils.

6.2.2 DETUMBLING CONTROL MODE

There are 2 detumbling modes implemented on-board. First is by default stored in the microprocessor on the purchased ISIS iMTQ board, and the second one is developed by the team and will be executed from the OBC. Following the P-POD deployment, the ISIS detumbling will be turned on. In the subsequent mission phases, the detumbling developed by the team will be performed.

In both detumbling modes, the angular rate will be monitored by the gyro, and the data will be sent to the ground where it will be analyzed. On the basis of the analysis performed on Earth, the TC will be sent to stop detumbling. Therefore, no autonomous detumbling termination is incorporated.

6.2.2.1 The B-Dot Algorithm

The B-Dot is the simplest algorithm used for decelerating the satellite's rotational motion. It is commonly used for detumbling after the P-POD deployment. In this section, the B-Dot algorithm implemented on the OBC is presented. The commanded magnetic dipole, \mathbf{m}_{ctrl} , is calculated using the magnetic field time derivative, $\dot{\mathbf{B}}$, calculated in the body frame and the magnetometer measurement, \mathbf{B} :

$$\mathbf{m}_{\text{ctrl}} = -k \frac{\dot{\mathbf{B}}}{\|\mathbf{B}\|^2} \quad (6.33)$$

Note that the magnetometer measurements need to be converted to SI units, namely [T]. To calculate the magnetic field time derivative, the high pass filter is used which substantially reduce the power consumption.

	PW-Sat2	Critical Design Review	
	2016-11-30		
	Phase C	Attitude Determination and Control System	

This computation method is recommended over the simple discrete time derivative. Therefore, the $\dot{\mathbf{B}}$ term calculated in the current time step i , is given by:

$$\dot{\mathbf{B}}_i = e^{-f_c \Delta t} \dot{\mathbf{B}}_{i-1} + f_c (\mathbf{B}_i - \mathbf{B}_{i-1}) \quad (6.34)$$

where f_c denotes the cut-off frequency in [rad/s] and Δt is the time step.

At $t = 0$, the previous magnetic field time derivative is set to $\mathbf{0}_{3 \times 1}$, and the previous magnetometer measurement is set to the current magnetic field measurement. Therefore, $\dot{\mathbf{B}}_0$ is $\mathbf{0}_{3 \times 1}$ as well. However, this does not influence the control law performance.

After the simulation campaign, the constants for the B-Dot were chosen as follows:

$$k = 2.879 \cdot 10^{-5} \text{ Nm/s}$$

$$f_c = 0.2 \text{ rad/s}$$

$$\Delta t = 0.2 \text{ s}$$

6.2.3 SUN POINTING CONTROL MODE

In Sun Pointing mode, spin stabilization is used in order to make the direction of rotation axis less sensitive to disturbance torques. In this section, the control law is presented.

6.2.3.1 Sun Pointing Algorithm

By spinning the satellite's around its X axis and controlling its direction so that it points towards the Sun, the deployed solar panels' plane is perpendicular to the Sun direction. The concept is presented in the figure below.

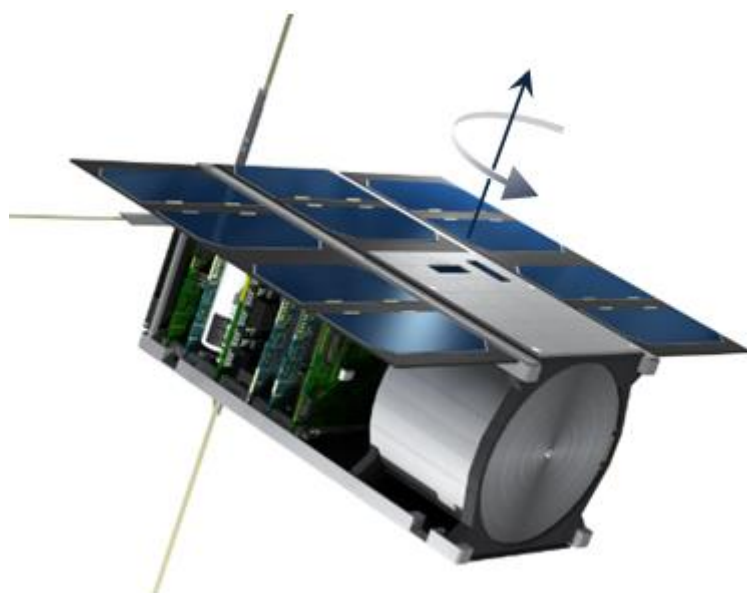


Figure 6-2 Spin stabilization around the satellite's X axis

	PW-Sat2	Critical Design Review	
	2016-11-30		
	Phase C	Attitude Determination and Control System	

The control law for spin stabilization in [6] was modified in order to account for Sun Pointing:

$$\mathbf{T}_{\text{comm}} = k_K \tilde{\mathbf{h}} + k_p e_{h,x} \begin{bmatrix} 1 \\ 0 \\ 0 \end{bmatrix} + k_n \mathbf{D} \boldsymbol{\omega}_{s/i} \quad (6.35)$$

where

$$\tilde{\mathbf{h}} = \mathbf{h}_{\text{comm}} - \mathbf{h} = \mathbf{I}(\mathbf{s}_b \|\boldsymbol{\omega}_{\text{comm}}\| - \boldsymbol{\omega}) \quad (6.36a)$$

$$e_{h,x} = h_{\text{comm}} - h_x = I_{xx} \|\boldsymbol{\omega}_{\text{comm}}\| - I_{xx} \omega_x \quad (6.36b)$$

Below the description of each term in Equations 6.35 and 6.36 is presented.

h̃	error between the satellite's commanded and current angular momentum vector expressed in the satellite's body frame
h_{comm}	commanded satellite's angular momentum vector expressed in the satellite's body frame
h	current satellite's angular momentum vector expressed in the satellite's body frame
I	inertia matrix calculated in the satellite's body frame
s_b	Sun vector in the body frame, obtained using the estimated Sun sensor angles and SS frame orientation
ω_{comm}	commanded satellite's angular rate relative to the ECI inertial frame expressed in the satellite's body frame
ω	current satellite's angular rate expressed in the satellite's body frame, equal the estimated angular rate
e_{h,x}	error between satellite's commanded and current angular momentum component along the satellite's X axis expressed in the satellite's body frame
h_{comm}	norm of the commanded satellite's angular momentum vector; it is the norm of the vector h_{comm}
h_x	X component of current satellite's angular momentum vector expressed in the satellite's body frame, assuming products of inertia equal 0
ω_x	X component of current satellite's angular rate expressed in satellite's body frame
D	selection matrix, $\mathbf{D} = \text{diag}(0,1,1)$
k_K	angular momentum gain
k_p	precession damping gain
k_n	nutation damping gain

Based on the set of simulations, control gains were chosen empirically, so that:

$$k_K = 4 \cdot 10^{-3}, k_p = 4 \cdot 10^{-3}, k_n = -10^{-4}$$

	PW-Sat2	Critical Design Review	
	2016-11-30		
	Phase C	Attitude Determination and Control System	

Satellite's commanded angular rate is defined in the satellite's body frame:

$$\boldsymbol{\omega}_{\text{comm}} = [5 \quad 0 \quad 0]^T \text{ deg/s}$$

The chosen value of the spin represents a trade-off between the gyroscopic stabilization, and the chosen time step Δt . The time step Δt corresponds to the control update frequency of $1/\Delta t$. Note that when the spin increases, the satellite rotation axis is more stable in the inertial frame, thus it is robust to the disturbance torques. On the other hand, when the satellite's spin increases, the time step should decrease. For the higher angular rate and fixed time step, the angular difference between two iterations is greater, which increases the errors of the propagated states in the Kalman filter. Also, the approximation in Eq. 6.16 is less accurate. Furthermore, the innovation and state covariance in eclipse increases faster which can reach very high values. This can cause numerical problems due to some matrix being close to singular. The simulations have shown that the satellite is stable with the angular rate of 5 deg/s. For this spin rate, the control update frequency of 1 Hz has proved to be sufficient. While reduction in the time step would result in increase in sensors noise, the time step is not meant to decrease. For these reasons, the spin rate of 5 deg/s and the control update frequency of 1 Hz have been chosen.

It is crucial that the moment of inertia around X axis in the satellite's body frame, I_{xx} , is the largest one. The rotational motion is stable only if the body spins around the largest or the smallest principal axis of inertia. For PW-Sat2, the products of inertia are negligible, therefore, the satellite's body frame can be treated as the principal frame. If the body spins around its intermediate axis of inertia, the motion will be unstable. According to PW-Sat2 current CAD model, the moments of inertia around satellite's X and Y axes are very close, even when the solar panels are deployed. In the configuration with the solar panels deployed, the inertia in the satellite's body frame is given by:

$$\mathbf{I} = \begin{bmatrix} 15456 & 7 & 24 \\ 7 & 14745 & -30 \\ 24 & -30 & 6479 \end{bmatrix} \text{ kg} \cdot \text{mm}^2$$

which gives the I_{xx}/I_{yy} ratio equal to 1.048. Note that this is the most favourable configuration with the solar panels deployed.

Although, the simulation results show that the ratio of 1.048 is sufficient, it is recommended, that the ratio between the moments of inertia around X and Y axes is not smaller than 1.1, giving the safety range for differences between modelled and real mass distribution:

$$I_{xx}/I_{yy} \geq 1.1$$

	PW-Sat2	Critical Design Review	
	2016-11-30	Attitude Determination and Control System	
	Phase C		

7 SIMULATION RESULTS

The simulation software developed in Matlab is described in the PDR documentation. There are two changes with respect to the architecture presented there:

- SGP4 orbit propagator was added, which replaced the J2 model
- IGRF12 model replaced the IGRF11 model

In the table below, input parameters constant for each simulation are presented. The time corresponds to the approximated launch date, which is set to the early December 2016. Orbit parameters have been updated, so that they match SSO circular orbit with an altitude of 575 km and LTDN 10:30. The simulation results for the detumbling mode are presented in the PDR and are not replicated here, since the B-dot architecture remains the same. Only the results for the Sun Pointing mode are presented here, due to the design changes.

Two Sun Pointing simulation results are presented. First corresponds to the initialization of the algorithm just after leaving the eclipse, and the second one initializes few iterations before entering the eclipse. The initial mean anomalies are presented below:

- Scenario 1: Initial mean anomaly: 88 deg
- Scenario 2: Initial mean anomaly: -44 deg

Note that the first scenario is the most favourable one, since the ADCS algorithms have the longest time to converge. The second case is the least favourable one, since the estimator does not have enough time to converge and shortly after the initialization acts as a propagator, which increases the state and residual covariance significantly. Nevertheless, it is shown that the estimator is able to recover and finally converges.

Initial attitude is set to random with the uniform distribution on the whole attitude sphere. Initial angular rates are generated using the Gaussian distribution with the mean value corresponding to the expected value following the successful detumbling. Note that no waiting for the SS Sun capture is included. Therefore, when at $t = 0$, the attitude is such that the Sun is not within the SS FoV, the initial attitude is generated once again, until the Sun is within the SS FoV.

Table 7-1 presents the simulation parameters.

Table 7-1 Simulation's parameters

Parameter	Value	Unit
Time:		
GMT time: 5.12.2017, 12:00	-	-
iteration time for Sun Pointing mode	1	s

	PW-Sat2	Critical Design Review	
	2016-11-30		
	Phase C	Attitude Determination and Control System	

Satellite

satellite's center of mass wrt geometrical center: X, Y, Z	6, -7, 8	mm
diagonal elements of inertia matrix: Ixx, Iyy, Izz	15456, 14745, 6479	kg mm ²
off-diagonal elements of inertia matrix: Ixy, Ixz, Iyz	7, 24, -30	kg mm ²

Sun Synchronous Orbit

altitude	575	km
eccentricity	1e-4	-
initial RAAN	49.7	deg
initial argument of perigee	0	deg

Initial Attitude & Angular Rate (SBRF wrt ECI):

yaw, pitch, roll	uniform distribution on the whole attitude sphere	-
initial angular rate for Sun Pointing mode (X, Y, Z)	Gaussian with $\mu = 0.1$ and $\sigma = 0.02$	deg/s

Magnetorquers:

nominal magnetic dipole for X, Y rods	0.2	Am ²
nominal magnetic dipole for Z aircore	0.24	Am ²

Environment:

IGRF12 order for true model	10th	-
atmospheric drag coefficient	2.2	-
solar constant	1363	W/m ²

Sensors:

gyro noise	0.3 (σ)	deg/s
gyro constant bias	0	deg/s
magnetometer noise	300 (σ)	nT
Sun sensor noise (both angles)	0.5 (σ)	deg
Sun sensor FoV	55 (half-cone)	deg

7.1.1 CASE 1

In the figures below, the results for the case 1 are presented.

In the Figure 7-1 the satellite's angular rate is presented. The satellite reaches the demanded angular rate around the X axis within 0.3 orbit, assuming no interruption by the eclipse. In the eclipse, the controller is turned off, hence some greater oscillations on Y and Z axes in eclipse.

Pointing accuracy outside eclipse is at the order of 2°, see Figure 7-2. Outside eclipse, the pointing error is approximately 5°, but when the satellite leaves eclipse, the attitude is rapidly corrected.

On the basis of the Figure 7-3, the magnetorquers are not saturated in the initial phase of the Sun Pointing. Note that in the eclipse, the commanded dipole equals 0.

	PW-Sat2	Critical Design Review	
	2016-11-30		
	Phase C	Attitude Determination and Control System	

Sun angles and the angular rate estimation errors are presented in the Figure 7-4. 3-sigma bounds are shown to determine whether the filter has converged and its outputs can be used by the controller. The estimation error is determined as a difference between the ‘true’ value and the estimated value. Note that the true value is available only in the simulation, thus allows to assess the filter performance in the simulation environment. When the filter has converged, the Sun angles are estimated with accuracy of 0.8 deg (3-sigma). The angular rate on X axis is estimated with the accuracy of 0.22 deg/s and on the Y and Z axes the accuracy is 0.14 deg/s. Slightly greater estimation error along X axis is due to the lack of the angle information about the satellite X axis (the Sun sensor outputs only 2 angles).

In eclipse, the estimation accuracy is corrupted due to the Sun sensor outage. The filter uses only the gyro measurements, but there is no update from the Sun sensor. The Sun angles estimation error grows exponentially, but the filter rapidly recovers when the satellite leaves the eclipse.

Note that the Sun angles estimation accuracy is also corrupted in the initial phases of the Sun pointing. This is due to the Sun directly above the Sun sensor’s head, which corresponds to the latitude angle of 0°, and the Sun Pointing error of 25°. The filter also recovers rapidly from this configuration.

The innovation presented in Figure 7-5 suggests that the observation and prediction equations are modeled correctly, because the innovation lies within 3-sigma bounds of the innovation covariance. Also note that the innovation 3-sigma bounds match the 3-sigma values of the measurements. In the initial phases of the Sun Pointing, the innovation of the Sun angles is equal 0, which indicates that there is no Sun sensor measurements. This suggests that the Sun left the SS FoV, due to the initial satellite’s angular rate.

	PW-Sat2	Critical Design Review	
	2016-11-30		
	Phase C	Attitude Determination and Control System	

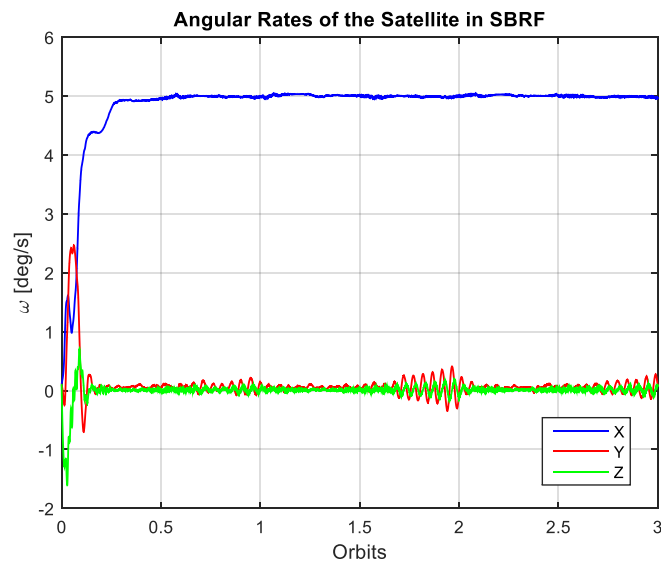


Figure 7-1 Case 1: Satellite's angular rate in SBRF

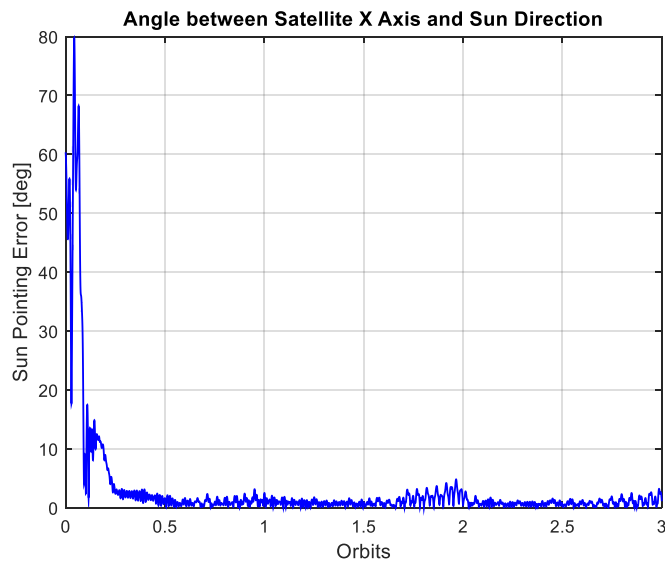


Figure 7-2 Case 1: Sun Pointing Error

	PW-Sat2	Critical Design Review	
	2016-11-30		
	Phase C	Attitude Determination and Control System	

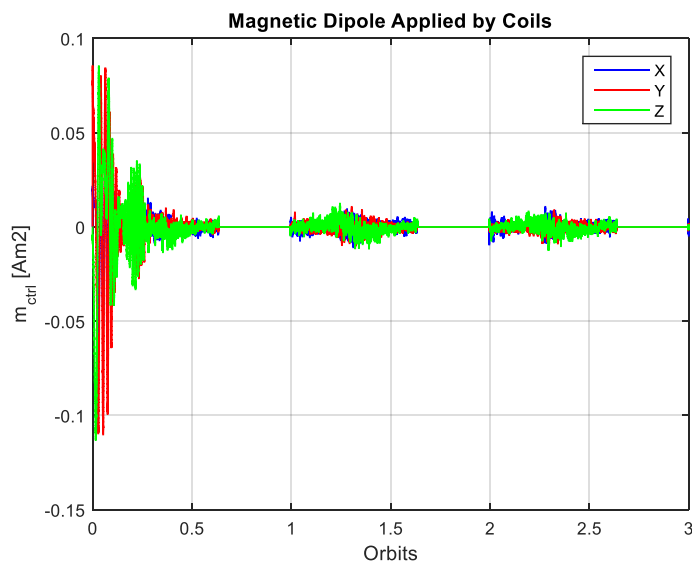


Figure 7-3 Case 1: Control magnetic dipole

	PW-Sat2	Critical Design Review	
	2016-11-30		
	Phase C	Attitude Determination and Control System	

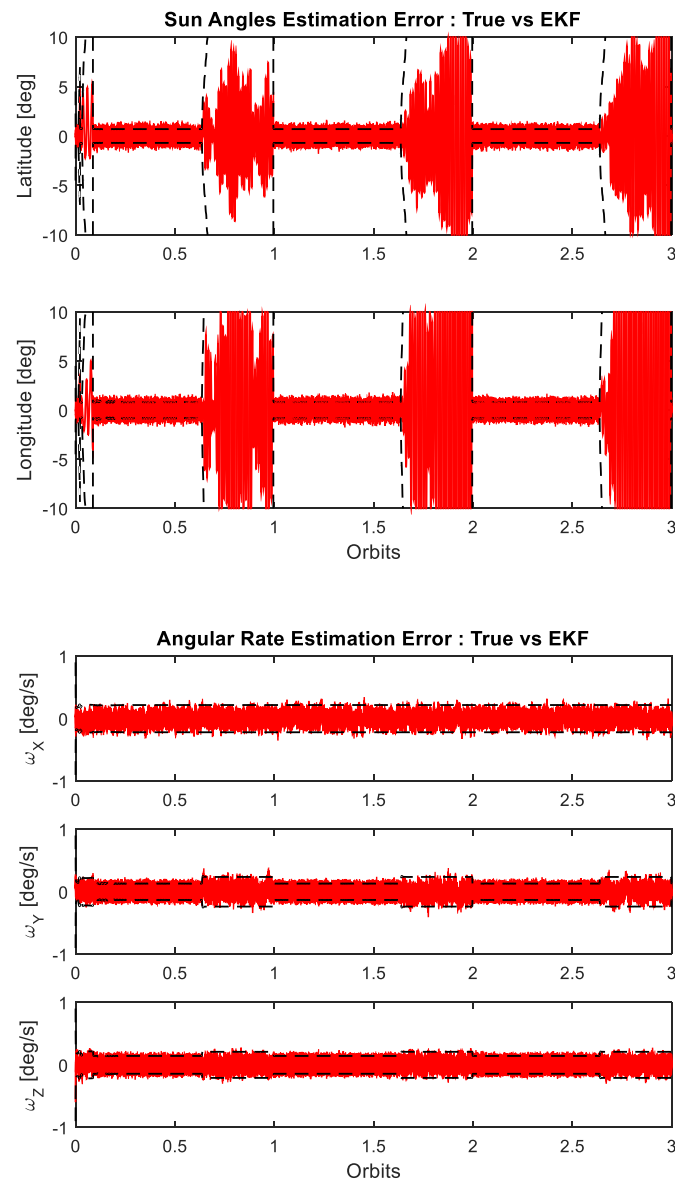


Figure 7-4 Case 1: EKF performance. Sun angles and angular rate estimation errors

	PW-Sat2	Critical Design Review	
	2016-11-30		
	Phase C	Attitude Determination and Control System	

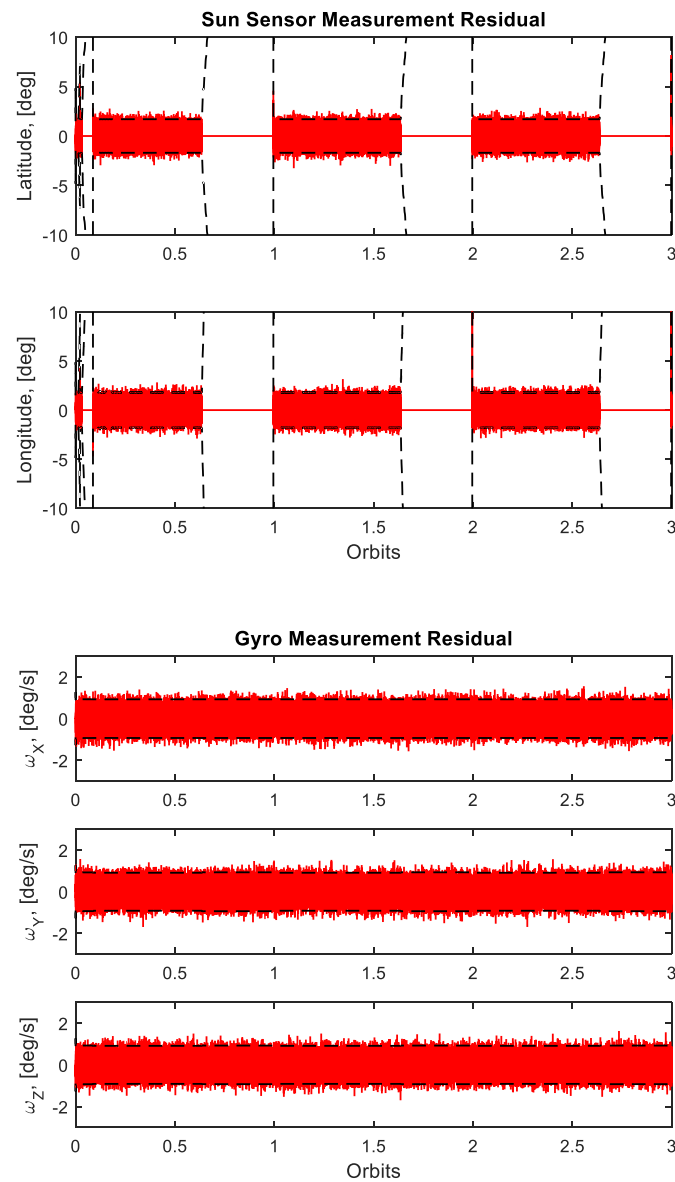


Figure 7-5 Case 1: EKF performance. Sun angles and angular rate residuals (innovations)

	PW-Sat2	Critical Design Review	
	2016-11-30	Attitude Determination and Control System	
	Phase C		

7.1.2 CASE 2

In the figures below, the results for the case 2 are presented.

The filter is initialized just before entering the eclipse. This time is too short for the controller to stabilize the rotation axis so that it points towards the Sun. The attitude control is turned off and the Sun sensor measurement is not updated. When the satellite leaves eclipse, the filter does not converge quickly due to the Sun being directly above the Sun sensor. This results in larger errors in predicted measurements, which can be seen in the Figure 7-10.

Also note that due to the large attitude errors, the magnetic coils are saturated, when the satellite leaves the eclipse, see Figure 7-8.

The estimation errors lies outside the 3-sigma bounds when the latitude angle is equal 0° . The filter diverges, and the estimate error is larger. Note however, that the state covariance is affected as well, which is an indication of the inconsistency of the data.

Eventually, the satellite is stabilized with the same accuracy as in the case 1. This scenario shows that the estimator is robust for unfavorable initialization moment and temporal sensor outage.

	PW-Sat2	Critical Design Review	
	2016-11-30		
	Phase C	Attitude Determination and Control System	

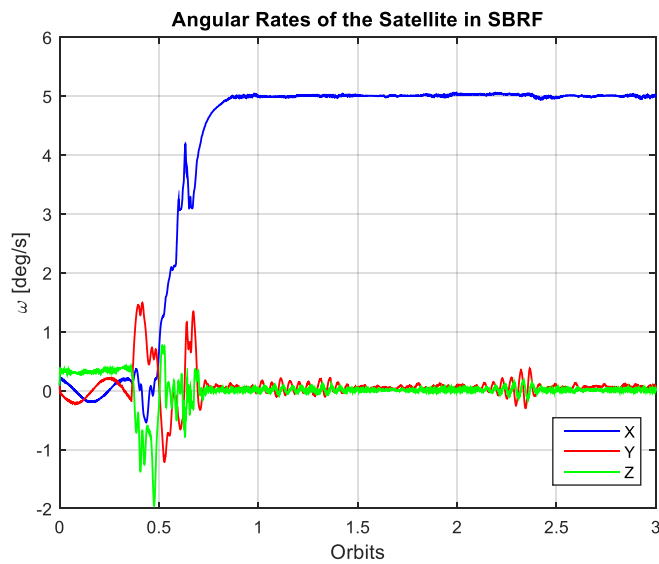


Figure 7-6 Case 2: Satellite's angular rate in SBRF

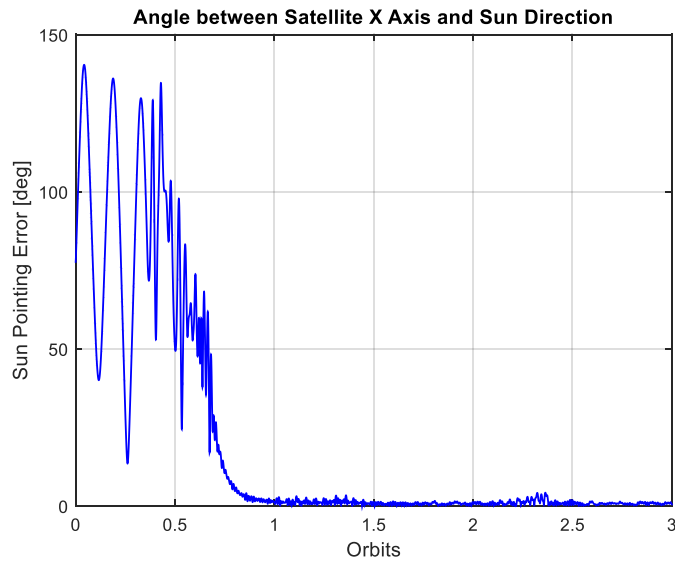


Figure 7-7 Case 2: Sun Pointing Error

	PW-Sat2	Critical Design Review	
	2016-11-30		
	Phase C	Attitude Determination and Control System	

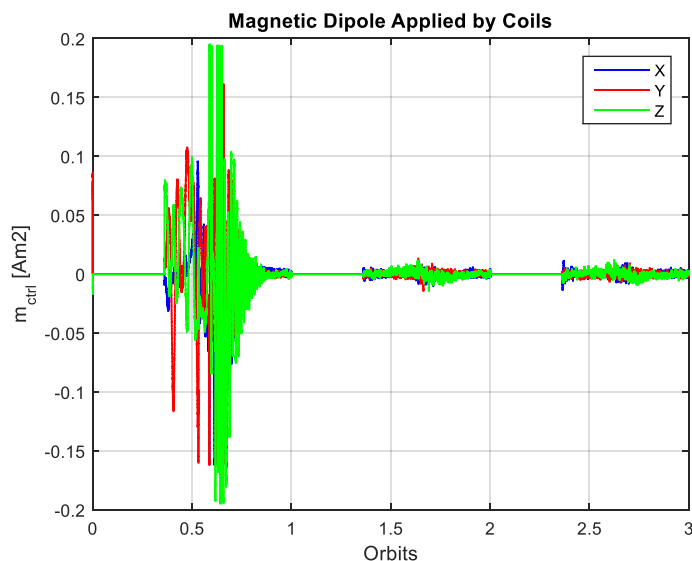


Figure 7-8 Case 2: Control magnetic dipole

	PW-Sat2	Critical Design Review	
	2016-11-30		
	Phase C	Attitude Determination and Control System	

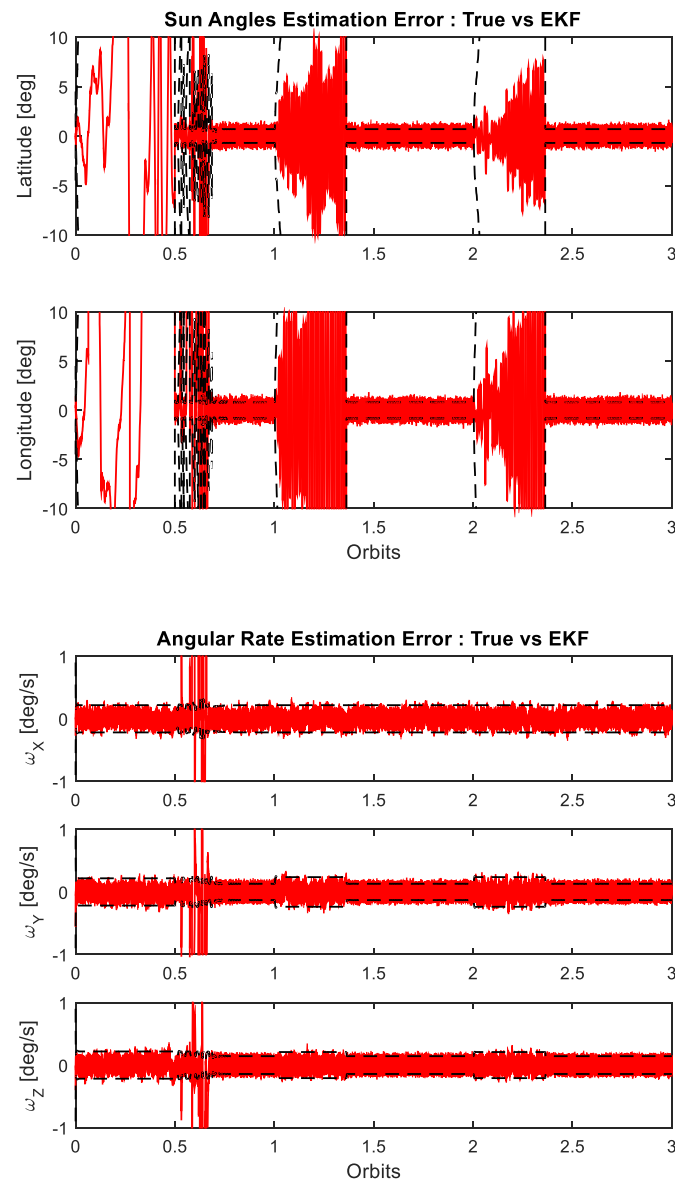


Figure 7-9 Case 2: EKF performance. Sun angles and angular rate estimation errors

	PW-Sat2	Critical Design Review	
	2016-11-30		
	Phase C	Attitude Determination and Control System	

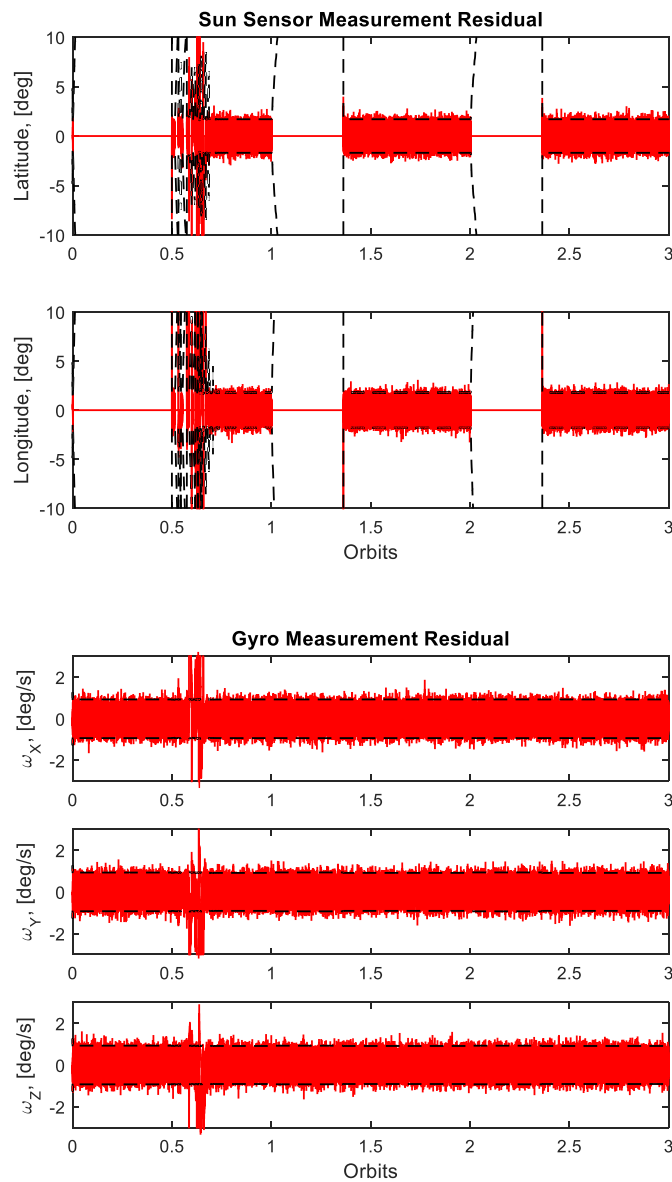


Figure 7-10 Case 2: EKF performance. Sun angles and angular rate residuals (innovations)

	PW-Sat2	Critical Design Review	
	2016-11-30	Attitude Determination and Control System	
	Phase C		

8 ADCS TEST CAMPAIGN

This chapter describes tests to be performed under the ADCS Test Campaign. Since ADCS is a complex system which contains several hardware and software components, to simplify the tests description it was divided into several sub-chapters:

- Hardware Testing
 - Sensors
 - Sun Sensor
 - Gyroscopes
 - Magnetometer
 - Actuators
 - Magnetotorquers
- Software Testing
 - Matlab
 - C

8.1 HARDWARE TESTING

All of the hardware components had been purchased from external various providers. All of the hardware components has a flight heritage. Therefore the test campaign is limited to the functional tests. All the launch provider required testing, such as vibrations, thermal-vacuum will be performed on the integrated satellite.

8.1.1 SENSORS

The ADCS sensors are located on the various electronics components. Magnetometers are part of iMTQ board, Sun sensor is located on the CubeSat wall and connected to the PLD board, where the gyroscopes are also placed

8.1.1.1 Sun Sensor

The Sun sensor device will be tested for its functional characteristics. The device is available in flight version only, therefore it should be always tested in cleanroom.

Functional Test Description

At the beginning of the functional test the device should be assembled with its wires connector, as shown in Figure 8-1. Next step will be connecting it to the PLD board and mounting on the test stand (Figure 8-2). The test stand were prepared for the Sun sensor device developed by the team. It allows 2-axis rotation powered with two step engines. To perform the test properly the Sun simulator is also required. The Sun sensor device will be checked in the whole range of angles.

	PW-Sat2	Critical Design Review	
	2016-11-30		
	Phase C	Attitude Determination and Control System	

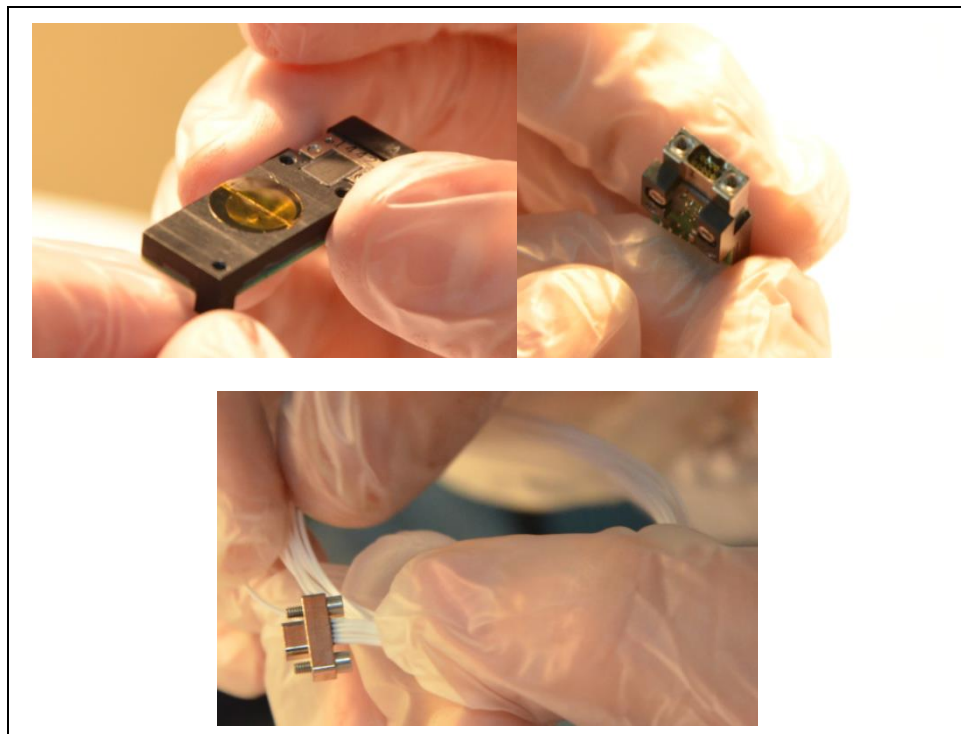


Figure 8-1Reference Sun Sensor wiring test

	PW-Sat2	Critical Design Review	
	2016-11-30		
	Phase C	Attitude Determination and Control System	

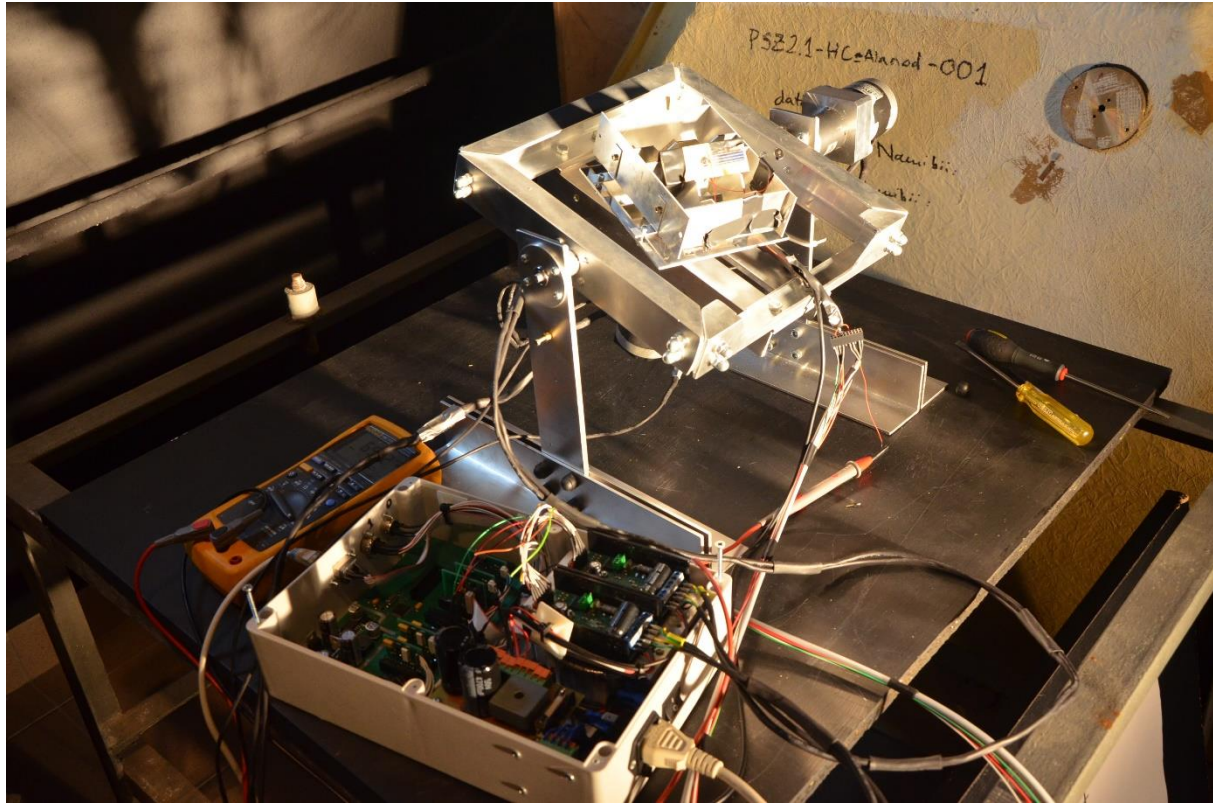


Figure 8-2 Sun Sensor test stand

8.1.1.2 Gyroscopes

The gyroscopes will be mounted on PLD board and will be controlled by OBC. In order to perform the test PLD board is required. The functional test can be divided into three phases:

- Static test,
- Dynamic test,
- Temperature test.

The static and dynamic tests will be performed at Rzeszów University of Technology. The test table (Figure 8-3) is much more precise than the gyroscopes used on board PW-Sat2. The table allows rotation in two axes.

	PW-Sat2	Critical Design Review	
	2016-11-30	Attitude Determination and Control System	
	Phase C		



Figure 8-3 Test table at Rzeszów University of Technology

The static test requires to keep the PLD board with the gyroscopes mounted on the table for 7 days. Then the data will be analyzed and compared with datasheet.

Dynamic test full option will be leaving the gyroscopes at 5 deg/s speed running for 7 days. The alternative option is to leave it for 24 hours, if the full options will be not possible due to logistics reasons.

The temperature test will be performed in order to compare the bias with datasheet. For the test gyroscopes will be tested in the temperature limits declared in its datasheets. The FM pieces will be tested only in the temperatures range requested by LP.

8.1.1.3 Magnetometers

The magnetometers are mounted on the iMTQ board. Only FM is available, therefore any tests should be performed in the cleanroom.

In order to properly test the magnetometers magnetic test stand (Helmholtz cage) is required. Since the team does not have an access to one, the test will be limited to check its polarization by checking the magnetometers response to the solid magnet in its area.

8.1.2 ACTUATORS

The actuators used for PW-Sat2 satellite are magnetorquers mounted on iMTQ board. Only FM is available, therefore any tests should be performed in the cleanroom.

	PW-Sat2	Critical Design Review	
	2016-11-30		
	Phase C	Attitude Determination and Control System	

In order to properly test the magnetic actuators Helmholtz cage is required, as well as for magnetometers. Since the team does not have an access to one, the test will be limited to check the power and communication with OBC.

8.2 SOFTWARE

The ADCS software contains the simulation environment and GNC algorithms developed in Matlab and the code in C that will be integrated with the rest of OBC software. The algorithms in C are rewritten from Matlab.

8.2.1 MATLAB

In order to test the ADCS algorithms developed in Matlab environment the simulation software is required. The simulation software were developed also by the team and contains:

- Time constrains (date and hour of simulation)
- Satellite dynamics and kinematics
- SGP4 orbit propagator using the TLE data
- Possibility of setting initial attitude and angular rate
- IGRF12 Earth's Geomagnetic Field model
- Sensors and actuators error models
- Disturbance torques, such as aerodynamic, gravity gradient, solar radiation pressure
- ADCS Guidance, Navigation and Control algorithms

Different GNC algorithms were tested in the simulation through the development process and the above list presents all the features that can be simulated in the environment developed by the team. Not all the features are required to simulate in the final system architecture, however use of a well-developed simulation environment might be valuable in the future.

Some of the parts of the simulator (IGRF, SGP4) were already validated and verified compared to available tools (www.ngdc.noaa.gov, <https://celestrak.com/>). However, the whole simulation environment should be checked. The MatLab simulation code was checked step-by-step by the ADCS team. Additionally, similar test was performed externally by an external reviewer from ABM Space company. As the final validation ad verification test, the ADCS team would like to test the algorithm in alternative software simulation environment used by associated companies. Possibilities are being investigated. C language

In order to test the ADCS software implemented on OBC limited test options are available.

- Physical test – place the satellite in Helmholtz cage and check the response of the actuators to the input sensors parameters. This test is not possible due to logistics problems, the team does not have an access to required facilities.

	PW-Sat2	Critical Design Review	
	2016-11-30		
	Phase C	Attitude Determination and Control System	

- Software in the loop – requires development of additional software to simulate the environment. The time required to develop the software might influence the project timeline, since its require the work hours which at the moment are limited in order to fit other priorities.
- Outputs analysis – is it possible, as an alternative to other test options, to give a certain input parameters from the sensors (only as inputs to the software) and analyze the outputs which will be the power to actuators.

	PW-Sat2	Critical Design Review	
	2016-11-30	Attitude Determination and Control System	
	Phase C		

9 CONCLUSIONS

In this document, the proposed ADCS architecture in Phase B was refined and verified. Attitude determination and estimation algorithms were tested with greater than expected sensors' noise. Control algorithms for spin stabilization and detumbling were implemented as well and tested, assuming certain set of errors.

Simulations results presented in chapter 7 prove that proposed ADCS design is feasible. The architecture of the navigation filter was simplified which eliminates the need to store the SGP4 orbit propagator, IGRF and Sun position models onboard. With the addition of the Sun sensor, the photodiodes are no longer necessary which simplifies the hardware design. Sun Pointing spin controller is robust for many sources of errors and disturbances and achieves the accuracy of the order of 2° outside eclipse. The actual pointing errors are expected to be slightly larger but still within the required limits, due to the large margin.

Modified estimation filter is robust for temporal sensor outage and unfavorable configuration with the Sun being directly above the Sun sensor. The Sun sensor normal was decided to be rotated by 25° with respect to the satellite's X axis to ensure that the latitude angle is safely away from 0° in the nominal configuration.

	PW-Sat2	Critical Design Review	
	2016-11-30	Attitude Determination and Control System	
	Phase C		

10 FUTURE WORK

During the project development different ADCS architectures were investigated by the team. At the time of writing this report (November 2016), the ADCS architecture converges to its final state. Only some minor changes are expected to be made in the final system, for example in the Kalman Filter design due to the reasons stated in this chapter.

From the algorithm design point of view, the filter convergence counter thresholds needs to be specified. Sensors tests are undergoing and the initial results indicate that the sensors performance matches the values in the sensors documentations, thus the measurement covariance matrix, \mathbf{R} , in the EKF is not expected to change significantly. The Monte Carlo simulations will be run to assess the filter performance, but the initial set of 100 simulations indicate that the design is very robust, always achieving Sun pointing configuration with 2° accuracy.

As the Algorithm in the Loop simulation in Matlab gives satisfactory results, the team is going to rewrite all the developed algorithms into C programming language. The software in the loop tests on the Personal Computer and Processor in the Loop, run on the evaluation board of the OBC processor, tests are going to be performed. The ADCS will start to work with closer cooperation with the OBC team who is responsible for OBC software development and integration.

Additionally, more and more hardware tests are going to be performed in order to understand the characteristic behavior of the chosen sensors, e.g. to check if the sensors do not behave in the unexpected way in some specific moments of operation. The aim of this work period is to identify potential problems with the sensors and eventually modify the software so that it takes some special cases into account. It is also predicted, that during this period of work, some sensors characteristics will be understood in a better way and thus their simulation model might be improved. This might result in a slight Kalman Filter modifications. Another test for the Kalman Filter implemented in the hardware is expected to be performed. A 2 DoF (variable pitch and roll) platform with a sun-simulating lamp will be used for this purpose.

The team will also specify the ADCS telemetry and telecommand data structure. They are expected to be as simple as possible in order to reduce the workload and mission complexity.

	PW-Sat2	Critical Design Review	
	2016-11-30		
	Phase C	Attitude Determination and Control System	

Appendix A COORDINATE SYSTEMS

In this document, three Cartesian coordinate systems are used. These are: ECI inertial frame, orbital frame and satellite's body frame denoted with subscripts i , o and s , respectively.

A.1 ECI – EARTH CENTRED INERTIAL

Fixed, inertial coordinate system $O_i x_i y_i z_i$ which origin coincides with the Earth's center of mass. The $O_i z_i$ axis is collinear with the Earth's axis of rotation and points towards North Pole. The $O_i x_i y_i$ plane coincides with the Earth's equatorial plane, the $O_i x_i$ axis is fixed at the vernal equinox and the $O_i y_i$ axis completes the right handed cartesian coordinate system. ECI inertial frame is pseudo inertial, i.e. its origin accelerates and the axes change their orientation in space due to the Sun and Moon perturbations. However, these effects can be neglected in most navigation applications.

A.2 ORF – ORBITAL REFERENCE FRAME

The origin and the axes orientation of the orbital frame $O_o x_o y_o z_o$ depend on the satellite's position on orbit. Its origin O_o coincides with the satellite's body frame origin O_s . The $O_o z_o$ axis points toward the center of the Earth, O_i . The $O_o x_o$ axis lies in the orbital plane and is collinear with the satellite's velocity vector for circular orbits. The $O_o y_o$ axis completes the right handed coordinate system $O_o x_o y_o z_o$ and is perpendicular to the orbital plane.

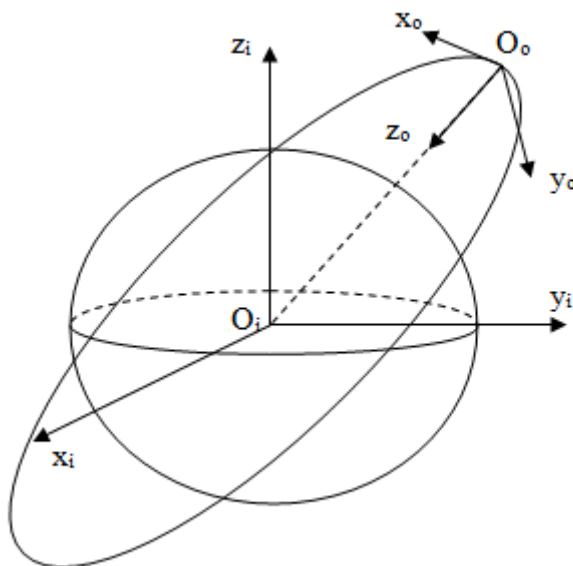


Figure A-1 ECI inertial and ORF orbital coordinate systems

	PW-Sat2	Critical Design Review	
	2016-11-30		
	Phase C	Attitude Determination and Control System	

A.3 SBRF – SATELLITE'S BODY REFERENCE FRAME

The SBRF coordinate system $O_s x_s y_s z_s$ is fixed with reference to the satellite. The origin O_s coincides with the satellite's center of mass. The $O_s x_s$ axis is perpendicular to the deployed solar panels and points outwards. The $O_s z_s$ axis is parallel to the deployed solar panels' plane and points towards the communication antennas. The $O_s y_s$ axis completes the right handed coordinate system $O_s x_s y_s z_s$. In the figure below, the SBRF's origin is moved away from the satellite for clarity.

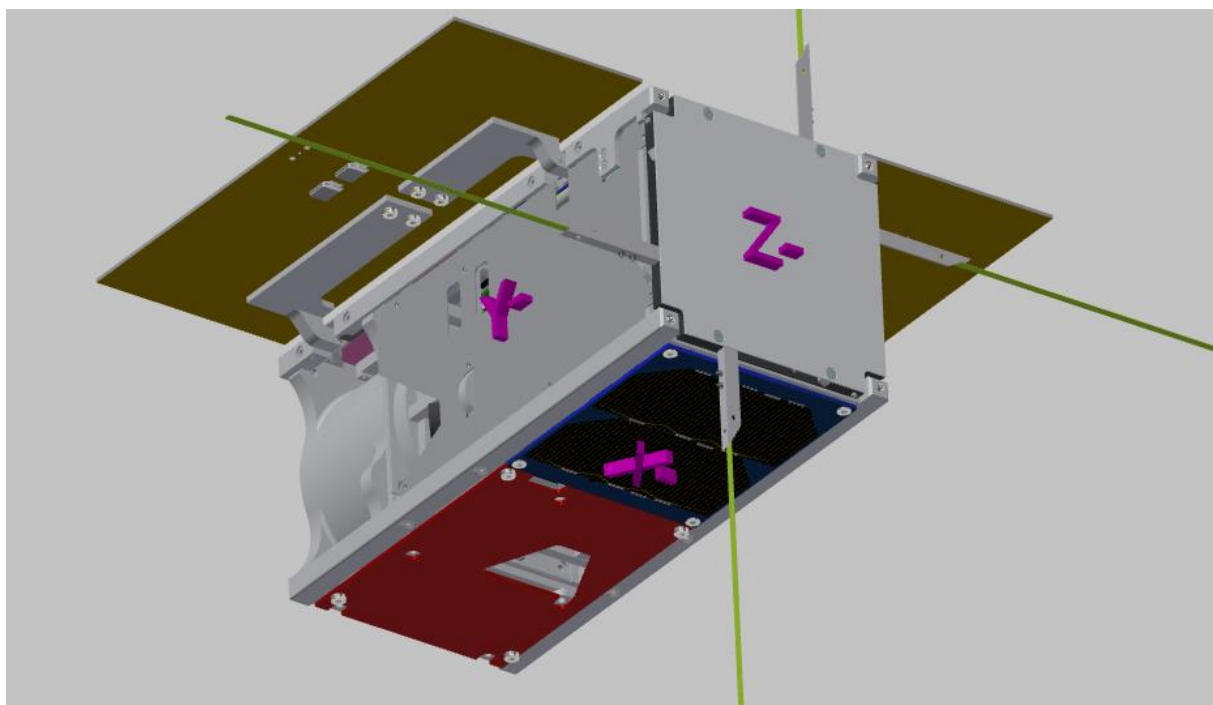


Figure A-2 Body axes definition [X-;Y-;Z-]

	PW-Sat2	Critical Design Review	
2016-11-30			
Phase C	Attitude Determination and Control System		

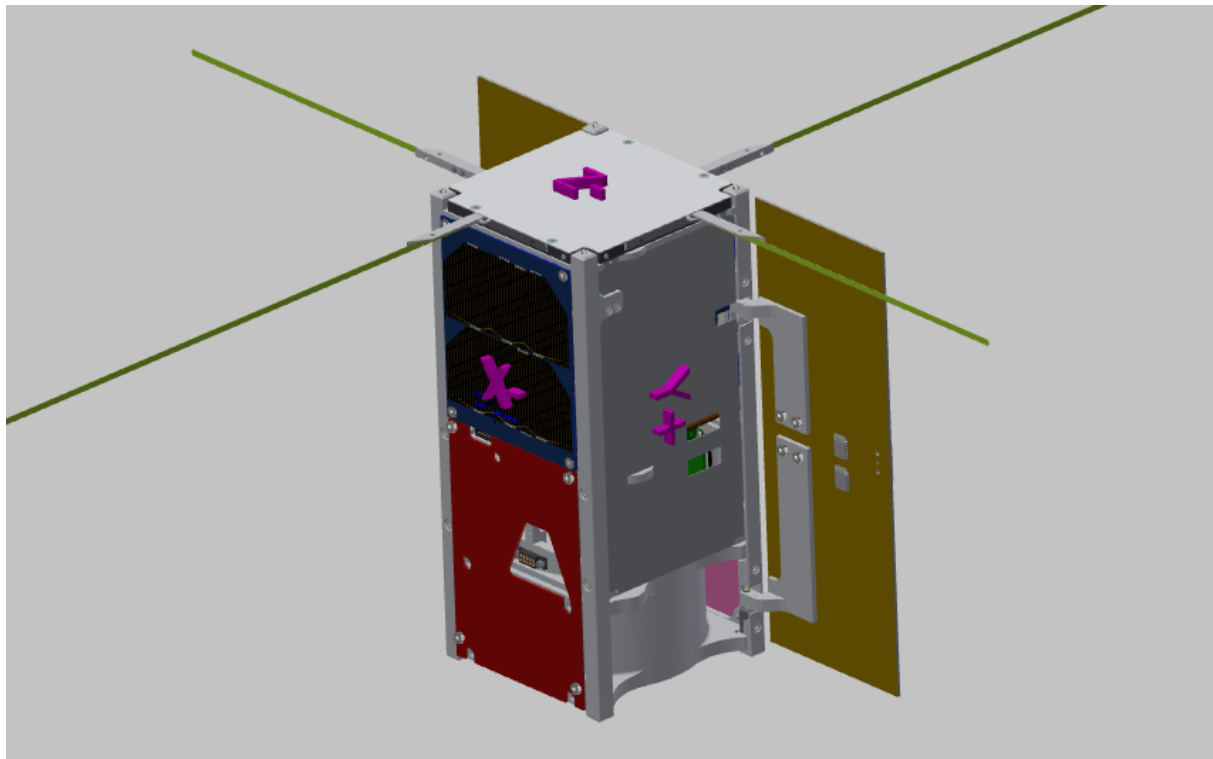


Figure A-3 Body axes definition [X-;Y+;Z-]

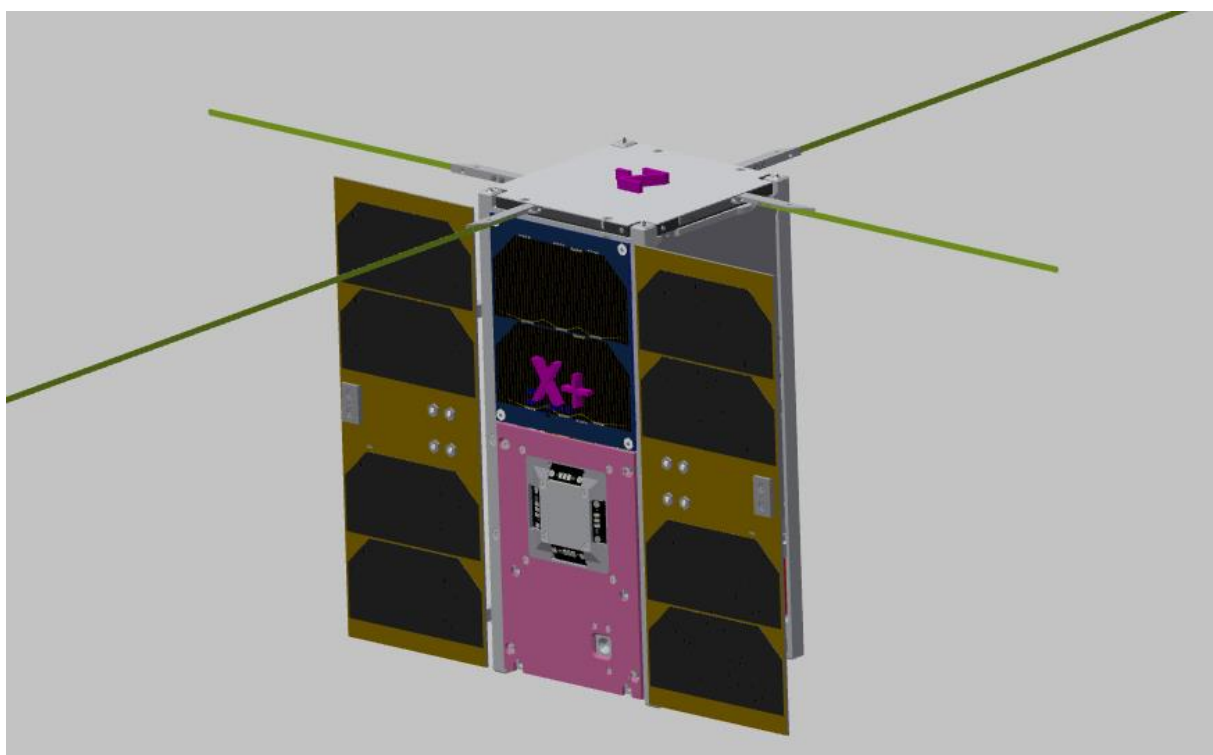


Figure A-4 Body axes definition [X+;Z-]

	PW-Sat2	Critical Design Review	
	2016-11-30		
	Phase C	Attitude Determination and Control System	

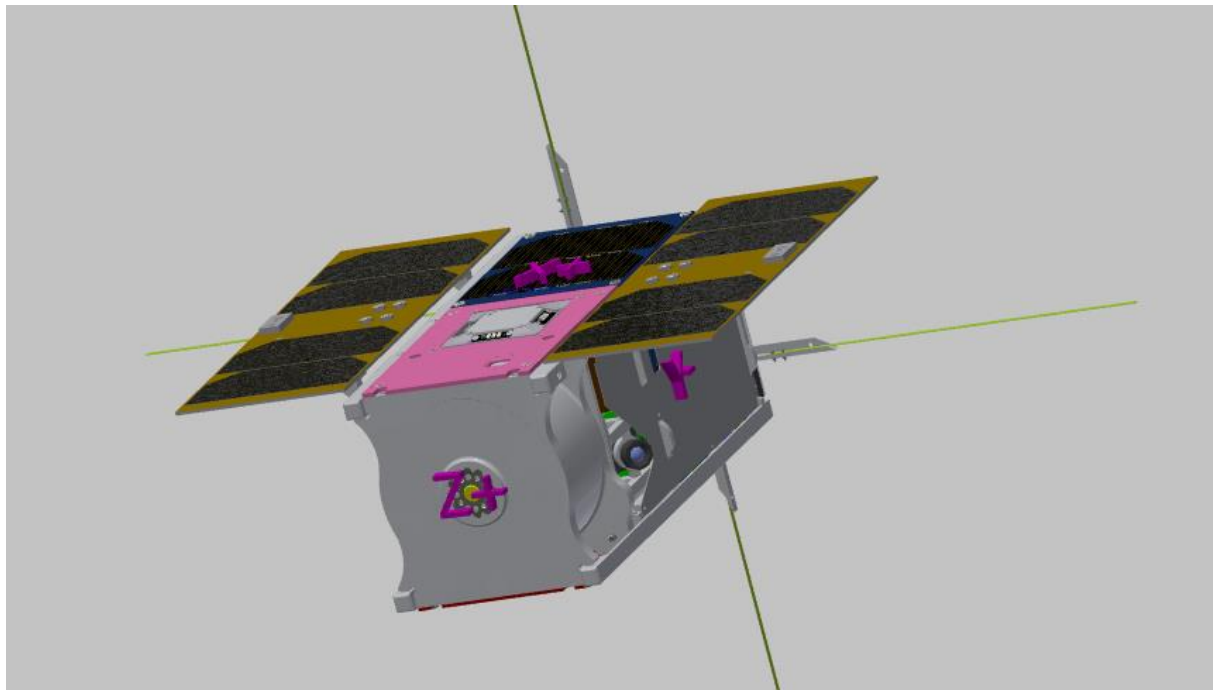


Figure A-5 Body axes definition [X+;Y-;Z+]